Mon. Not. R. Astron. Soc. **360,** 974–992 (2005) doi:10.1111/j.1365-2966.2005.09087.x

A statistical study of 233 pulsar proper motions

G. Hobbs,[1,2]★ D. R. Lorimer,[2] A. G. Lyne[2] and M. Kramer[2]

[1]*Australia Telescope National Facility, CSIRO, PO Box 76, Epping, NSW 1710, Australia*
[2]*University of Manchester, Jodrell Bank Observatory, Macclesfield, Cheshire SK11 9DL*

Accepted 2005 April 5. Received 2005 April 4; in original form 2004 December 8

ABSTRACT

We present and analyse a catalogue of 233 pulsars with proper motion measurements. The sample contains a wide variety of pulsars including recycled objects and those associated with globular clusters or supernova remnants. After taking the most precise proper motions for those pulsars for which multiple measurements are available, the majority of the proper motions (58 per cent) are derived from pulsar timing methods, 41 per cent using interferometers and the remaining 1 per cent using optical telescopes. Many of the one-dimensional (1D) and two-dimensional (2D) speeds (referring to speeds measured in one coordinate only and the magnitudes of the transverse velocities, respectively) derived from these measurements are somewhat lower than earlier estimates because of the use of the most recent electron density model in determining pulsar distances. The mean 1D speeds for the normal and recycled pulsars are 152(10) and 54(6) km s^{-1}, respectively. The corresponding mean 2D speeds are 246(22) and 87(13) km s^{-1}. PSRs B2011+38 and B2224+64 have the highest inferred 2D speeds of $\sim$1600 km s^{-1}. We study the mean speeds for different subsamples and find that, in general, they agree with previous results. Applying a novel deconvolution technique to the sample of 73 pulsars with characteristic ages less than 3 Myr, we find the mean three-dimensional (3D) pulsar birth velocity to be 400(40) km s^{-1}. The distribution of velocities is well described by a Maxwellian distribution with 1D rms $\sigma = 265$ km s^{-1}. There is no evidence for a bimodal velocity distribution. The proper motions for PSRs B1830−08 and B2334+61 are consistent with their proposed associations with the supernova remnants W41 and G114.3+0.3, respectively.

Key words: stars: kinematics – pulsars: general.

1 INTRODUCTION

Neutron stars are high-velocity objects. From observations of radio pulsars, it has long been known (Gunn & Ostriker 1970) that as a population they are generally moving much faster than their presumed progenitor population, the massive OB stars. While the astrophysical applications of a large sample of pulsar velocities are manyfold, most importantly the physical mechanism for the high velocities is not well understood. Lai, Chernoff & Cordes (2001) have summarized the various discussed causes for high pulsar velocities. These mechanisms, in general, only predict a limited range of velocities, so that a large sample of pulsar velocities can in principle be used to test the mechanisms.

Pulsar velocities are determined from measurements of their proper motion and distance. Prior to the recent publication by Hobbs et al. (2004; hereafter Paper I) approximately 138 pulsar proper motions had been measured, with 68 having values greater than 2σ. Most millisecond pulsar proper motions had been obtained using timing methods (e.g. Nice & Taylor 1995; Toscano et al. 1999b; Wolszczan et al. 2000; Freire et al. 2003). The poor rotational stability observed for young pulsars[1] (referred to as timing noise) affected early measurements of proper motions using timing methods; for these, interferometers had been used to obtain the proper motions (for example, Lyne, Anderson & Salter 1982; Bailes et al. 1990a; Harrison, Lyne & Anderson 1993; Fomalont et al. 1997; Brisken et al. 2002). In Paper I we described a new method, based on the modelling and removal of timing noise from the timing residuals of young pulsars using harmonically related sinusoids, that allowed accurate proper motions to be determined using standard timing methods. These proper motions were shown to be consistent with

★E-mail: hob044@kepler.atnf.csiro.au

[1] We use the words 'young' and 'old' throughout this paper to refer to pulsars with small and large characteristic ages, $\tau_c = P/2\dot{P}$. The characteristic age assumes that the current rotational period of the pulsar is much greater than the initial period and that pulsar slow-down is due to a constant magnetic dipole field. The characteristic age may not be a good estimation of the true age if dipole braking is not strictly followed.

proper motion measurements obtained using interferometers. We obtained proper motions for 301 pulsars with 164 having values greater than 2σ or with an uncertainty less than 15 mas yr^{-1} in at least one coordinate. For 87 of these pulsars, these provide more precise proper motions than the earlier measurements.

Direct distance measurements have only been obtained for a small number of pulsars. The majority of distances are estimated from the dispersion measure and a Galactic electron density model. Using the Taylor & Cordes (1993; hereafter TC93) model, Lyne & Lorimer (1994) found the mean pulsar birth velocity[2] to be 450(90) km s^{-1}. Recently, Cordes & Lazio (2002; hereafter CL02) provided an updated model which, on average, predicts somewhat smaller distances than TC93 which will clearly have an impact on the calculated velocities. Hereafter, we designate the velocities derived from the two models as $V^{\rm TC}$ and $V^{\rm CL}$.

Clearly, with these new proper motion determinations and a new electron density model it is productive to revisit the statistics of pulsar velocities. In Section 2, we describe the sample of proper motions used in this work which combines new results published in Paper I with other proper motion values in the literature. In Section 3, we highlight the effect of using the CL02 electron density model to obtain pulsar distances and velocities. In Section 4 we examine the statistical properties of various subsamples of the observed sample. Following a brief discussion of the motion of pulsars in the Galactic plane in Section 5, we estimate the 3D birth speed distribution of non-millisecond pulsars in Section 6. Finally, in Section 7, we summarize our main results and conclusions.

2 THE PROPER MOTION SAMPLE

Proper motions were selected from the literature with more precise measurements taking precedence if multiple measurements exist for a specific pulsar. In practice, these proper motions were obtained from the Australia Telescope National Facility (ATNF) pulsar catalogue[3] (Manchester et al. 2005) or from Paper I. These proper motion measurements all have values greater than 2σ or have an uncertainty less than 15 mas yr^{-1}. As discussed in Paper I, for a pulsar lying in the ecliptic plane it is not possible, using timing methods, to obtain a precise estimate of its proper motion in ecliptic latitude. Therefore, only the longitudinal component of the proper motion has been measured for many of the pulsars in the sample. The timing solutions for the 87 pulsars obtained from Paper I have been updated using the most recent data available from the Jodrell Bank Observatory data archive. The timing solutions were obtained in an identical manner to that described in Paper I. The most recent observations used in these timing solutions are from 2004 February.

The resulting sample of 233 proper motions is provided in Table 1. As detailed in the caption, Table 1 also includes the 2D speed (often referred to as the transverse speed), $V_{\rm T}^{\rm CL} = \mu_{\rm tot} D^{\rm CL}$, and the difference in 2D speed between CL02 and TC93, $V_{\rm T}^{\rm TC} - V_{\rm T}^{\rm CL}$.

The sample contains a wide variety of pulsars including 'normal', recycled (defined here as pulsars with spin-periods, $P < 0.1$ s and spin-down rates, $\dot{P} < 10^{-17}$), 'young' (those pulsars with characteristic ages $\tau_{\rm c} < 3$ Myr) and pulsars associated with supernova remnants or globular clusters. In our sample, 58 per cent of the proper motions were determined using timing methods, 41 per cent using interferometers and the remaining 1 per cent using optical telescopes. In Fig. 1 we plot the positions and proper motions on the sky. The apparent motions with respect to the Galactic plane seen in this figure are discussed in detail in Section 5.

Our sample includes 12 pulsars that are situated within globular clusters and for which a 2D speed can be determined. The mean 2D speed for this subsample is 149(8) km s^{-1}. However, this includes the proper motion of the globular clusters as well as the pulsars themselves. For 47 Tucanae, removing the *Hipparcos* measurement of the cluster proper motion of $\mu_\alpha = 5.3(6)$ mas yr^{-1} and $\mu_\delta = -3.3(6)$ mas yr^{-1} (Odenkirchen et al. 1997) from the measured proper motions indicates that the intrinsic mean 2D speed of the 11 pulsars with measured proper motions in the cluster is 25(5) km s^{-1}. That the mean velocity of recycled pulsars in globular clusters is significantly lower than those moving in the Galactic potential is not surprising given the smaller escape velocity of the clusters compared to the Galaxy. For 47 Tucanae, for example, the escape velocity is $\sim$58 km s^{-1} (Webbink 1985). As the measured proper motion of a pulsar in a globular cluster is dominated by the cluster motion we will leave such pulsars out of the remaining discussion and analysis of this paper.

In Table 2 we tabulate for each pulsar: Galactic position, proper motion in Galactic latitude and longitude, height above the Galactic plane, speed perpendicular to the Galactic plane, characteristic age, $\tau_{\rm c} = P/2\dot{P}$ and surface magnetic field strength, $B_{\rm s} = 3.2 \times 10^{19} (P\dot{P})^{1/2}$ G. The effects of stellar motion and Galactic rotation have been removed from the proper motions given in this table. To do this, we assumed a flat Galactic rotation curve with galactocentric distance of the Sun, $\rm R_\odot = 8.5$ kpc and the Galactic rotation of the Sun, $\rm V_\odot = 225$ km s^{-1}. These are identical to the values used in the analysis by Harrison et al. (1993) and are similar to the current IAU standard of $\rm R_\odot = 8.5$ kpc and $\rm V_\odot = 220$ km s^{-1} (Kerr & Lynden-Bell 1986). Most suggested rotation curves of our Galaxy, e.g. Olling & Merrifield (1998), only deviate significantly from a flat rotation curves for distances from the Galactic centre <3 kpc. As none of the pulsars in our sample are within this region of the Galaxy, our assumption of a flat rotation curve does not significantly affect our results.

Similarly, we choose the same values for the peculiar motion of the Sun as Harrison et al. (1993) of 15.6 km s^{-1} in the direction of $l = 48\overset{\circ}{.}8$ and $b = 26\overset{\circ}{.}3$. This motion is close to the value of 13.4 km s^{-1} obtained by Dehnen & Binney (1997) using *Hipparcos* data. Software to carry out these conversions between equatorial (or ecliptic) and Galactic proper motions is available as part of the ATNF pulsar catalogue software package (Manchester et al. 2005). As the uncertainties in pulsar distances discussed in the next section are, on average, much larger than the effects of assuming a specific rotation curve and solar motion values, the resulting 1D and 2D speed distributions are unaffected by this correction. In the following, we therefore choose not to correct the samples for these small effects.

3 PULSAR DISTANCES

Model-independent distances to 22 pulsars within our sample are available from measurements of annual parallax. These distances are known to within 10 per cent accuracy and are listed in Table 3. Limits on the distances for a further 13 pulsars have been determined using H I absorption or by associations with globular clusters or supernova remnants (such limits are reviewed by Frail & Weisberg 1990). The distances to the remaining pulsars are estimated from their dispersion measures and a Galactic electron density model. The

[2] Throughout this paper, we will present the uncertainties on parameters as a value in parentheses after each quantity. The value represents the error (at the 68 per cent confidence level) in the least significant digit.

[3] http://www.atnf.csiro.au/research/pulsar/psrcat

Table 1. Pulsar proper motions. For each pulsar, the two components of its proper motion are provided followed by a flag stating whether these are given in celestial (C) or ecliptic (E) coordinates. The remaining columns provide the total proper motion, a reference for the measurement (see the end of the table for the full bibliographic reference), whether the proper motion was determined using interferometric (I), timing (T) or optical (O) means, the distance according to the CL02 distance model or from independent distance estimates if available, the magnitude of the transverse velocity assuming the CL02 or independent distance estimates (ind.) and the difference $\Delta V_{\rm T} = V_{\rm T}^{\rm TC} - V_{\rm T}^{\rm CL}$ between the velocities as measured assuming the CL02 and TC93 distances.

PSR	$\mu_{\rm long}$ (mas yr^{-1})	$\mu_{\rm lat}$ (mas yr^{-1})	Coord.	$\mu_{\rm tot}$ (mas yr^{-1})	Ref.	Obs. type	Dist. (kpc)	$V_{\rm T}^{\rm CL}$ (km s^{-1})	$\Delta V_{\rm T}$ (km s^{-1})
B0011+47	19.3(18)	−19.7(15)	C	27.6(17)	1	I	1.56	204	34
B0021−72C	5.2(5)	−3.2(4)	C	6.1(5)	2	T	5.00	145	ind.
B0021−72D	3.8(4)	−2.4(4)	C	4.5(4)	2	T	5.00	107	ind.
B0021−72E	6.2(5)	−2.7(5)	C	6.8(5)	2	T	5.00	161	ind.
B0021−72F	4.6(5)	−2.9(6)	C	5.4(6)	2	T	5.00	128	ind.
B0021−72G	4.2(14)	−3.7(12)	C	5.6(14)	2	T	5.00	133	ind.
B0021−72H	5.1(12)	−3.6(12)	C	6.2(12)	2	T	5.00	147	ind.
B0021−72I	4.9(16)	−3.9(19)	C	6.3(18)	2	T	5.00	149	ind.
B0021−72J	5.35(13)	−3.42(15)	C	6.35(14)	2	T	5.00	150	ind.
B0021−72N	6.8(13)	−1.1(14)	C	6.9(14)	2	T	5.00	164	ind.
J0024−7204O	4.6(11)	−2.9(9)	C	5.4(11)	2	T	5.00	128	ind.
J0024−7204U	5.1(7)	−4.5(7)	C	6.8(7)	2	T	5.00	161	ind.
J0034−0534	5.5(15)	−31(9)	E	31(9)	3	T	0.54	79	65
B0031−07	−8(12)	–	E	–	3	T	0.41	–	–
B0037+56	3(10)	−7(13)	E	8(13)	3	T	3.05	116	54
B0114+58	7(5)	17(6)	E	18(6)	3	T	2.23	190	−8
J0134−2937	8(3)	−21(5)	E	22(5)	3	T	0.56	58	127
B0136+57	−11(5)	−19(5)	C	22(5)	4	I	2.88	300	1
B0138+59	7(12)	–	E	–	3	T	2.19	–	–
B0144+59	−3.8(19)	10(3)	E	11(3)	3	T	2.22	116	−16
B0149−16	3.1(12)	−27(2)	C	27(2)	1	I	0.51	66	36
B0203−40	–	75(35)	C	–	5	T	0.58	–	–
J0218+4232	3(3)	−4(7)	E	5(6)	3	T	2.67	63	75
B0254−53	–	70(15)	C	–	5	T	0.73	–	–
B0301+19	6(7)	−37(4)	C	37(5)	6	I	0.62	109	58
B0320+39	16(6)	−30(5)	C	34(6)	4	I	1.01	163	77
B0329+54	17.0(3)	−9.5(4)	C	19.5(4)	7	I	1.06	98	ind.
B0331+45	−4(3)	5(8)	E	6(7)	3	T	1.64	47	13
B0353+52	6(3)	−9(6)	E	11(6)	3	T	2.78	145	102
B0355+54	9.20(18)	8.2(4)	C	12.3(3)	8	I	1.10	64	57
B0402+61	23(7)	61(12)	E	65(12)	3	T	2.12	653	287
B0410+69	−4(5)	−12(7)	E	13(7)	3	T	1.18	73	24
J0437−4715	121.457(9)	−71.449(9)	C	140.914(9)	9	T	0.14	94	ind.
B0447−12	10(11)	–	E	–	3	T	1.89	–	–
B0450−18	12(8)	–	C	–	10	I	2.36	–	–
B0450+55	52(6)	−17(2)	C	55(6)	4	I	0.67	175	31
B0458+46	−8(3)	8(5)	C	11(5)	4	I	1.39	72	20
B0523+11	30(7)	−4(5)	C	30(7)	4	I	3.11	442	650
B0525+21	–	7(9)	C	–	4	I	1.61	–	–
B0531+21	−13(2)	7(3)	C	15(3)	11	O	2.00	142	ind.
J0538+2817	−30(6)	–	E	–	3	T	1.23	–	–
B0540+23	19(7)	12(8)	C	22(8)	4	I	2.06	215	154
B0559−05	18(8)	−16(7)	C	24(8)	4	I	3.93	447	411
B0609+37	5(3)	5(12)	E	7(9)	3	T	0.87	29	21
J0613−0200	2.0(4)	−7.0(10)	C	7.3(10)	12	T	1.71	59	17
B0611+22	−4(5)	−3(7)	C	5(6)	4	I	2.08	49	63
J0621+1002	3.5(3)	−0.3(9)	C	3.5(4)	13	T	1.36	23	9
B0621−04	0(10)	–	E	–	3	T	2.78	–	–
B0626+24	−7(12)	2(12)	C	7(12)	4	I	2.24	74	81
B0628−28	−44.6(9)	20(3)	C	48.7(13)	1	I	1.45	335	162

Table 1 – *continued*

PSR	$\mu_{\rm long}$ (mas yr^{-1})	$\mu_{\rm lat}$ (mas yr^{-1})	Coord.	$\mu_{\rm tot}$ (mas yr^{-1})	Ref.	Obs. type	Dist. (kpc)	$V_{\rm T}^{\rm CL}$ (km s^{-1})	$\Delta V_{\rm T}$ (km s^{-1})
J0633+1746	138(4)	97(4)	C	169(4)	14	O	0.16	128	ind.
B0643+80	19(3)	−1(3)	C	19(3)	4	I	1.55	140	164
B0656+14	44.1(6)	−2.4(3)	C	44.2(6)	15	I	0.29	59	ind.
B0655+64	−6(5)	−8(8)	E	10(8)	3	T	0.49	23	0
J0711−6830	−15.7(5)	15.3(6)	C	21.9(6)	12	T	0.86	90	19
B0736−40	−14.0(12)	−13(3)	C	19.0(17)	1	I	2.64	238	756
B0740−28	−29(2)	4(2)	C	29.3(2)	10	I	2.07	287	−25
J0751+1807	−0.2(10)	–	E	–	3	T	1.15	–	–
B0751+32	−4(5)	7(3)	C	8(4)	4	I	1.52	58	91
B0756−15	1(4)	4(6)	C	4(6)	1	I	2.95	56	15
B0809+74	24.02(9)	−44.0(4)	C	50.1(4)	7	I	0.43	102	ind.
B0818−13	9(9)	−47(6)	C	48(7)	10	I	1.99	453	105
B0820+02	5(11)	−1(8)	C	5(11)	4	I	1.01	24	10
B0823+26	61(3)	−90(2)	C	109(3)	6	I	0.36	186	ind.
B0833−45	−49.60(6)	29.80(10)	C	57.86(8)	16	I	0.29	80	ind.
B0834+06	2(5)	51(3)	C	51(4)	6	I	0.65	157	17
B0835−41	−2.3(18)	−18(4)	C	18(4)	1	I	1.60	137	225
B0906−17	27(11)	−40(11)	C	48(11)	4	I	0.91	207	−64
B0919+06	18.35(6)	86.56(12)	C	88.48(12)	17	I	1.20	503	ind.
B0940+16	–	9(11)	C	–	4	I	0.81	–	–
B0942−13	–	−22(14)	C	–	4	I	0.67	–	–
B0943+10	–	−21(12)	C	–	6	I	0.64	–	–
B0950+08	−2.09(8)	29.46(7)	C	29.53(8)	7	I	0.26	36	ind.
J1012+5307	2.4(2)	−25.2(2)	C	25.3(2)	18	T	0.41	49	13
J1022+1001	−16.3(6)	–	E	–	3	T	0.45	–	–
J1024−0719	−41(2)	−70(3)	C	81(3)	12	T	0.39	150	−15
B1039−19	−1(3)	14(5)	C	14(5)	1	I	1.48	98	113
J1045−4509	−5(2)	6.0(10)	C	7.8(15)	12	T	1.96	72	47
B1112+50	22(3)	−51(3)	C	56(3)	4	I	0.45	119	24
B1114−41	−1(5)	–	C	–	1	I	1.47	–	–
B1133+16	−74.0(4)	368.1(3)	C	375.5(4)	7	I	0.36	641	ind.
B1237+25	−106.82(17)	49.92(18)	C	117.91(18)	7	I	0.86	481	ind.
B1254−10	−6(8)	–	E	–	3	T	1.55	–	–
B1257+12	46.40(10)	−82.2(2)	C	94.39(19)	19	T	0.77	345	ind.
B1309−12	−1(6)	–	E	–	3	T	3.14	–	–
B1322+83	−53(20)	13(7)	C	55(20)	4	I	0.76	198	3
B1325−43	3(7)	54(23)	C	54(23)	1	I	1.34	343	243
B1426−66	−31(5)	−21(3)	C	37(5)	20	I	1.00	175	140
B1449−64	−16.0(10)	−21.3(8)	C	26.6(9)	20	I	2.08	262	−30
J1455−3330	5(6)	24(12)	C	25(12)	12	T	0.53	63	25
B1451−68	−39.5(4)	−12.3(3)	C	41.4(4)	20	I	0.45	88	ind.
B1508+55	−70.6(16)	−68.8(12)	C	98.6(15)	1	I	0.99	463	444
J1518+4904	4.6(6)	−8.1(6)	E	9.3(6)	3	T	0.63	28	3
B1534+12	1.340(10)	−25.05(2)	C	25.09(2)	21	T	0.95	113	−6
B1541+09	−7.3(10)	−4.0(10)	C	8.3(10)	1	I	3.49	137	−41
B1540−06	−17(3)	−4(3)	C	18(3)	1	I	0.72	61	37
B1552−31	−9(8)	–	E	–	3	T	2.33	–	–
B1556−44	1(6)	14(11)	C	14(11)	10	I	2.29	152	−47
J1603−2531	−10(4)	–	E	–	3	T	1.87	–	–
B1600−27	−21(11)	–	E	–	3	T	1.56	–	–
J1603−7202	−3.5(3)	−7.8(5)	C	8.5(5)	12	T	1.17	47	19
B1600−49	−30(7)	−1(3)	C	30(7)	20	I	5.10	725	−215
B1604−00	−1(14)	−7(9)	C	7(10)	6	I	0.67	22	−3
B1620−09	−17(10)	–	E	–	3	T	>50.00	–	–
B1620−26	−13.4(10)	−25(5)	C	28(5)	22	T	1.80	239	ind.

Table 1 – *continued*

PSR	$\mu_{\rm long}$ (mas yr^{-1})	$\mu_{\rm lat}$ (mas yr^{-1})	Coord.	$\mu_{\rm tot}$ (mas yr^{-1})	Ref.	Obs. type	Dist. (kpc)	$V_{\rm T}^{\rm CL}$ (km s^{-1})	$\Delta V_{\rm T}$ (km s^{-1})
J1640+2224	−0.1(3)	−13.3(7)	C	13.3(7)	19	T	1.16	73	2
J1643−1224	3.0(10)	−8(5)	C	9(5)	12	T	2.41	103	105
B1642−03	−3.7(15)	30.0(16)	C	30.2(16)	1	I	1.12	160	256
B1700−18	−9(11)	–	E	–	3	T	1.48	–	–
B1700−32	−31(14)	–	E	–	3	T	2.33	–	–
B1702−19	−66(5)	–	E	–	3	T	0.88	–	–
J1709+2313	−3.2(7)	−9.7(9)	C	10.2(9)	23	T	1.41	68	20
B1706−16	3(9)	0(14)	C	3(9)	10	I	0.83	12	6
J1713+0747	4.9(3)	−4.1(10)	C	6.4(7)	24	T	1.11	34	ind.
B1718−02	−1(4)	−26(5)	C	26(5)	1	I	2.51	309	357
B1718−32	0(5)	–	E	–	3	T	2.35	–	–
J1730−2304	19.9(6)	–	E	–	3	T	0.53	–	–
B1732−07	−2.4(17)	28(3)	C	29(3)	1	I	2.26	311	283
B1735−32	−3(13)	–	E	–	3	T	1.20	–	–
B1737+13	−22(3)	−20(3)	C	29(3)	1	I	1.48	203	452
J1744−1134	18.72(6)	−9.5(4)	C	20.99(19)	25	T	0.36	36	ind.
B1742−30	11(4)	–	E	–	3	T	1.91	–	–
B1745−12	3(6)	–	E	–	3	T	2.45	–	–
B1749−28	−4(6)	−5(5)	C	6(6)	10	I	1.23	35	9
B1754−24	−17(5)	–	E	–	3	T	4.40	–	–
B1756−22	−22(5)	–	E	–	3	T	3.57	–	–
B1757−24	2(9)	−3(9)	C	4(9)	26	I	5.22	99	−12
B1802−07	−5(6)	–	E	–	3	T	3.10	–	–
J1804−2717	2(4)	–	E	–	3	T	0.78	–	–
B1802+03	−12(6)	–	E	–	3	T	2.84	–	–
B1804−08	−5(4)	1(4)	C	5(4)	10	I	2.73	65	21
B1806−21	−5(7)	–	E	–	3	T	5.23	–	–
B1813−17	−9(11)	–	E	–	3	T	6.33	–	–
B1815−14	−12(9)	–	E	–	3	T	7.15	–	–
B1818−04	−10(3)	10(9)	E	14(7)	3	T	1.94	129	34
B1821+05	5(11)	−2(4)	C	5(11)	4	I	1.83	43	28
B1820−30A	2(2)	–	E	–	3	T	8.00	–	–
B1820−31	16(3)	–	E	–	3	T	1.29	–	–
B1821−24	−0.90(10)	−4.6(18)	C	4.7(18)	31	T	5.80	129	ind.
B1822+00	−18(10)	–	E	–	3	T	1.91	–	–
B1822−09	−13(11)	−9(5)	C	16(10)	10	I	0.88	67	9
B1822−14	12(14)	–	E	–	3	T	5.06	–	–
B1829−08	−3(4)	–	E	–	3	T	4.85	–	–
B1829−10	−13(6)	–	E	–	3	T	5.81	–	–
B1830−08	−30(3)	15(11)	E	34(6)	3	T	4.66	751	163
B1831−04	−1(8)	–	E	–	3	T	2.16	–	–
B1834−04	−2(5)	12(14)	E	12(14)	3	T	4.94	281	−18
B1839+56	−30(4)	−21(2)	C	37(4)	4	I	1.68	295	4
B1838−04	6(3)	−10(8)	E	12(8)	3	T	5.68	323	−29
B1842+14	−9(10)	45(6)	C	46(7)	4	I	2.19	478	9
B1841−04	−6(10)	–	E	–	3	T	2.92	–	–
B1841−05	7(5)	–	E	–	3	T	6.51	–	–
B1844−04	−3(6)	–	E	–	3	T	3.26	–	–
B1845−01	−1(6)	–	E	–	3	T	3.99	–	–
B1846−06	17(8)	–	E	–	3	T	3.41	–	–
B1848+13	−16(6)	−2(10)	E	16(7)	3	T	2.69	204	34
J1852−2610	−15(11)	–	E	–	3	T	1.75	–	–
B1855+02	−11(7)	–	E	–	3	T	7.98	–	–
B1855+09	−2.94(4)	−5.41(6)	C	6.16(6)	27	T	0.91	27	ind.
B1857−26	−19.9(3)	−47.3(9)	C	51.3(9)	28	I	2.00	486	ind.

Table 1 – *continued*

PSR	$\mu_{\rm long}$ (mas yr^{-1})	$\mu_{\rm lat}$ (mas yr^{-1})	Coord.	$\mu_{\rm tot}$ (mas yr^{-1})	Ref.	Obs. type	Dist. (kpc)	$V_{\rm T}^{\rm CL}$ (km s^{-1})	$\Delta V_{\rm T}$ (km s^{-1})
B1859+01	6(10)	–	E	–	3	T	2.79	–	–
B1900+05	−8(8)	–	E	–	3	T	4.66	–	–
B1900+06	−4(6)	−7(13)	E	8(12)	3	T	8.44	320	45
B1900−06	−2(8)	–	E	–	3	T	5.37	–	–
B1902−01	1(5)	9(14)	E	9(14)	3	T	6.01	256	38
B1904+06	−6(6)	−1(11)	E	6(7)	3	T	8.31	236	26
B1905+39	11(4)	11.0(10)	C	16(3)	4	I	2.24	170	−36
B1907+00	−2(6)	–	E	–	3	T	3.57	–	–
B1907+02	1(10)	–	E	–	3	T	4.94	–	–
B1907+10	−5(4)	8(8)	E	9(8)	3	T	4.18	178	6
J1909−3744	−9.6(2)	−35.6(7)	C	36.9(7)	29	T	0.46	80	86
J1911−1114	−6(4)	−23(13)	C	24(13)	12	T	1.22	139	42
B1911+13	−8(5)	−11(8)	E	14(8)	3	T	5.12	340	−3
B1911−04	7(13)	−5(9)	C	9(12)	4	I	2.79	119	18
B1913+10	1(3)	−7(6)	E	7(6)	3	T	6.27	208	−32
B1913+16	−2.56(6)	0.49(7)	C	2.61(7)	30	T	5.90	73	15
B1914+09	−9(4)	−1(7)	E	9(5)	3	T	2.94	125	−3
B1917+00	–	−1(10)	C	–	4	I	3.06	–	–
B1919+21	–	40(10)	C	–	10	I	1.09	–	–
B1924+16	3(8)	−16(13)	E	16(13)	3	T	5.83	442	145
B1929+10	94.03(14)	43.4(3)	C	103.56(18)	8	I	0.36	177	ind.
B1933+16	−1(3)	−13(3)	C	13(3)	10	I	5.61	346	143
B1935+25	−14(3)	−11(4)	E	18(4)	3	T	3.25	277	−42
B1937+21	−0.46(2)	−0.66(2)	C	0.80(2)	32	T	3.60	14	ind.
B1937−26	12(2)	−10(4)	C	16(3)	33	I	1.66	126	234
B1944+17	1(5)	−9(4)	C	9(5)	6	I	1.40	60	−23
B1943−29	19(9)	–	C	–	1	I	1.54	–	–
B1946+35	−12.6(6)	−0.7(6)	C	12.6(6)	4?	I	5.80	346	124
B1951+32	−24(4)	−8(3)	C	25(4)	34	I	2.50	296	ind.
B1952+29	–	−36(10)	C	–	6	I	0.70	–	–
B1953+29	−1.0(3)	−3.7(3)	C	3.8(3)	19	T	4.64	84	14
B1953+50	−23(5)	54(5)	C	59(5)	4	I	2.24	626	−123
B1957+20	−16.0(5)	−25.8(6)	C	30.4(6)	35	T	2.49	359	−138
B2000+40	−13(7)	−3(7)	E	13(7)	3	T	5.90	364	148
B2002+31	−5(8)	−10(11)	E	11(11)	3	T	7.50	391	75
B2011+38	−32.1(17)	−25(3)	C	41(2)	1	I	8.44	1624	891
B2016+28	−2.6(2)	−6.2(4)	C	6.7(4)	7	I	0.97	31	ind.
J2019+2425	−9.41(12)	−20.60(15)	C	22.65(15)	36	T	1.49	160	−62
B2020+28	−4.4(5)	−23.6(3)	C	24.0(4)	7	I	2.70	307	ind.
B2021+51	−5.23(17)	11.5(3)	C	12.6(3)	7	I	2.00	119	ind.
B2022+50	17(3)	14(3)	E	22(3)	3	T	2.34	244	−56
B2044+15	−13(6)	3(4)	C	13(6)	4	I	2.42	149	9
B2043−04	–	−7(8)	C	–	4	I	1.75	–	–
B2045−16	117(5)	−5(5)	C	117(5)	10	I	0.56	311	44
J2051−0827	5.3(10)	0(3)	C	5.3(11)	37	T	1.04	26	6
B2053+21	−5(6)	−1(9)	E	5(7)	3	T	2.43	58	−7
B2053+36	−3(7)	3(3)	C	4(6)	4	I	4.62	88	18
B2106+44	3.5(13)	1.4(14)	C	3.8(14)	1	I	4.96	89	6
B2110+27	−23(2)	−54(3)	C	59(3)	4	I	2.03	568	−179
B2111+46	7(12)	−11(13)	E	13(13)	3	T	4.53	279	28
B2113+14	–	−11(5)	C	–	4	I	4.17	–	–
J2124−3358	−14.0(10)	−47.0(10)	C	49.0(10)	12	T	0.27	63	−5
J2129−5721	7(2)	−4(3)	C	8(3)	12	T	1.36	52	45
J2145−0750	−12.37(6)	−6.8(8)	C	14.1(4)	40	T	0.50	33	ind.
B2148+63	14(3)	10(4)	C	17(4)	4	I	5.51	444	656

Table 1 – *continued*

PSR	$\mu_{\rm long}$ (mas yr^{-1})	$\mu_{\rm lat}$ (mas yr^{-1})	Coord.	$\mu_{\rm tot}$ (mas yr^{-1})	Ref.	Obs. type	Dist. (kpc)	$V_{\rm T}^{\rm CL}$ (km s^{-1})	$\Delta V_{\rm T}$ (km s^{-1})
B2148+52	7(3)	−5(3)	E	9(3)	3	T	4.62	197	45
B2154+40	17.8(8)	2.8(10)	C	18.0(9)	1	I	3.76	321	155
B2217+47	−12(8)	−30(6)	C	32(7)	6	I	2.22	337	35
B2224+65	144(3)	112(3)	C	182(3)	4	I	1.86	1605	121
J2229+2643	1(4)	−17(4)	C	17(4)	19	T	1.45	117	−2
B2227+61	8(10)	6(11)	E	10(11)	3	T	4.04	192	79
J2235+1506	15(4)	10(8)	C	18(6)	38	T	1.07	91	7
B2255+58	11(4)	−14(5)	E	18(5)	3	T	4.51	385	161
B2303+30	2(2)	−20(2)	C	20(3)	1	I	3.66	347	25
B2306+55	−15(8)	–	C	–	4	I	2.16	–	–
B2310+42	21.4(9)	−5.3(12)	E	22.0(10)	3	T	1.25	130	−31
J2317+1439	−1.7(15)	7(4)	C	8(4)	38	T	0.83	31	40
B2315+21	2(9)	–	E	–	3	T	0.95	–	–
J2322+2057	−17(2)	−18(3)	C	25(3)	39	T	0.80	95	−2
B2324+60	−18(5)	6(5)	E	19(5)	3	T	4.86	438	−4
B2327−20	74.7(19)	5(3)	C	75(2)	1	I	0.39	138	36
B2334+61	−7(12)	−8(13)	E	11(13)	3	T	3.15	164	−35
B2351+61	22(3)	6(2)	C	23(3)	4	I	3.43	374	−13

References: (1) Brisken et al. (2003a), (2) Freire et al. (2003), (3) Hobbs et al. (2004), (4) Harrison et al. (1993), (5) Siegman, Manchester & Durdin (1993), (6) Lyne et al. (1982), (7) Brisken et al. (2002), (8) Chatterjee et al. (2004), (9) van Straten et al. (2001), (10) Fomalont et al. (1997), (11) Wyckoff & Murray (1977) (12) Toscano et al. (1999b), (13) Splaver et al. (2002), (14) Caraveo et al. (1996), (15) Brisken et al. (2003b), (16) Dodson et al. (2003), (17) Chatterjee et al. (2001), (18) Lange et al. (2001), (19) Wolszczan et al. (2000), (20) Bailes et al. (1990a), (21) Konacki, Wolszczan & Stairs (2003), (22) Thorsett et al. (1999), (23) Lewandowski et al. (2004), (24) Camilo, Foster & Wolszczan (1994), (25) Toscano et al. (1999a), (26) Thorsett et al. (2002), (27) Kaspi, Taylor & Ryba (1994), (28) Fomalont et al. (1999), (29) Jacoby et al. (2003), (30) Weisberg & Taylor (2003), (31) Cognard & Lestrade (1997), (32) Cognard et al. (1995), (33) McGary et al. (2001), (34) Migliazzo et al. (2002), (35) Arzoumanian, Fruchter & Taylor (1994), (36) Nice, Splaver & Stairs (2001), (37) Doroshenko et al. (2001), (38) Camilo, Nice & Taylor (1996), (39) Nice & Taylor (1995), (40) Löhmer et al. (2004).

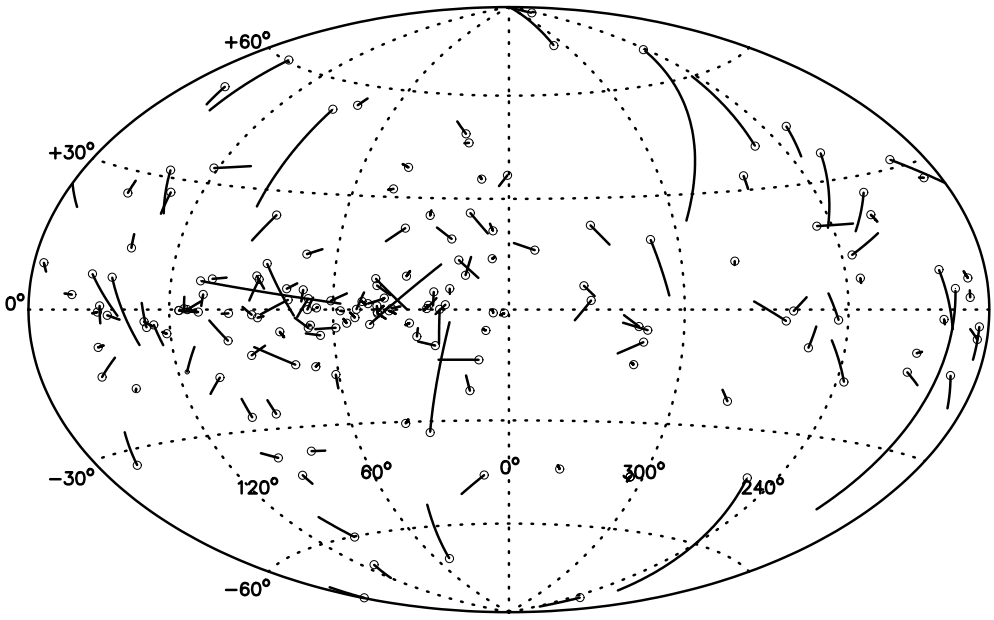

Figure 1. The Galactic motions of the pulsars in our sample. A pulsar is currently at the position indicated by a circle and the track indicates its motion for the last 1 Myr assuming no radial velocity.

TC93 model attempted to predict distances accurate to 25 per cent or better on average. The CL02 model purports to provide distances with a similar accuracy, CLO2 report that typical distance uncertainties are slightly less than 20 per cent). Extensive comparisons between the two models have been made (see, for example, Cordes & Lazio 2003; Kramer et al. 2003). Here, we emphasize that the two models are not entirely consistent and list major discrepancies for the pulsars considered in this paper in Table 4. With the CL02 model, only a lower limit of 50 kpc is provided for the distance to PSR B1620−09 (the TC93 model places this pulsar at 3.9 kpc). The

Table 2. Proper motions in Galactic coordinates. In column order, the table lists pulsar name, Galactic coordinates, proper motion in Galactic coordinates, the height above the Galactic plane, the velocity in this direction, $V_Z = \mu_b D \cos b$, the base-10 logarithms of the characteristic age and surface magnetic field strength.

PSR	l (°)	b (°)	μ_l (mas yr^{-1})	μ_b (mas yr^{-1})	Z (kpc)	V_Z (km s^{-1})	log[τ_c (yr)]	log[B_s (G)]
B0011+47	116.57	−14.64	18.4(18)	−20.8(16)	−0.39	−149	7.54	11.93
B0021−72C	305.99	−44.88	−1.4(5)	3.6(5)	−3.39	58	–	–
B0021−72D	305.94	−44.88	0.1(4)	3.1(4)	−3.39	50	–	–
B0021−72E	305.95	−44.87	−2.4(5)	3.0(5)	−3.39	48	8.76	8.78
B0021−72F	305.96	−44.88	−0.8(6)	3.4(6)	−3.39	55	8.81	8.62
B0021−72G	305.95	−44.88	−0.5(14)	4.3(13)	−3.39	69	–	–
B0021−72H	305.96	−44.89	−1.4(12)	4.1(12)	−3.39	66	–	–
B0021−72I	305.95	−44.88	−1.2(17)	4.4(19)	−3.39	71	–	–
B0021−72J	305.97	−44.89	−1.62(14)	3.84(15)	−3.39	62	–	–
B0021−72N	305.95	−44.88	−2.7(14)	1.3(14)	−3.39	21	–	–
J0024−7204O	305.96	−44.88	−0.8(11)	3.4(10)	−3.39	55	9.14	8.46
J0024−7204U	305.95	−44.89	−1.5(7)	5.0(7)	−3.39	81	8.86	8.81
J0034−0534	111.58	−68.08	−27(9)	15(3)	−0.50	14	9.78	7.99
B0037+56	121.53	−5.58	−6(12)	−2(11)	−0.30	−22	6.79	12.26
B0114+58	126.36	−3.47	10(6)	17(6)	−0.13	179	5.44	11.89
J0134−2937	230.38	−80.24	−8(5)	20(4)	−0.55	9	7.44	11.02
B0136+57	129.29	−4.06	−6(5)	−20(5)	−0.20	−272	5.61	12.24
B0144+59	130.13	−2.73	12(3)	4(3)	−0.11	42	7.08	11.36
B0149−16	179.42	−72.46	20.2(18)	−16.6(16)	−0.49	−12	7.01	12.02
J0218+4232	139.58	−17.54	−2(7)	2(4)	−0.80	22	8.68	8.63
B0301+19	161.22	−33.27	24(7)	−25(6)	−0.34	−61	7.23	12.13
B0320+39	152.26	−14.34	29(6)	−14(6)	−0.25	−65	7.88	12.15
B0329+54	145.07	−1.23	18.2(4)	3.5(4)	−0.02	18	6.74	12.09
B0331+45	150.42	−8.04	9(8)	−1(4)	−0.23	−10	8.76	10.65
B0353+52	149.17	−0.53	−8(6)	1(4)	−0.03	13	6.82	11.49
B0355+54	148.26	0.80	0.4(3)	13.5(4)	0.02	70	5.75	11.92
B0402+61	144.10	7.04	40(11)	54(9)	0.26	539	6.23	12.26
B0410+69	138.98	13.66	−3(7)	−11(7)	0.28	−60	7.91	11.24
J0437−4715	253.47	−41.95	75.456(9)	120.263(9)	−0.09	59	9.20	8.76
B0450+55	152.69	7.54	43(5)	32(5)	0.09	101	6.36	11.96
B0458+46	160.43	3.07	−12(5)	−1(4)	0.07	−5	6.26	12.28
B0523+11	192.77	−13.24	19(6)	23(7)	−0.71	330	7.88	11.21
B0531+21	184.63	−5.78	−14(3)	−7(3)	−0.20	−66	3.09	12.58
B0540+23	184.44	−3.32	−1(8)	23(8)	−0.12	224	5.40	12.29
B0559−05	212.27	−13.47	23(8)	9(8)	−0.92	163	6.68	11.86
B0609+37	175.52	9.09	7(12)	6(5)	0.14	24	7.90	11.13
J0613−0200	210.49	−9.30	7.8(10)	−1.3(6)	−0.28	−10	9.71	8.24
B0611+22	188.86	2.40	0(7)	−5(6)	0.09	−49	4.95	12.66
J0621+1002	200.64	−2.01	1.7(9)	3.6(5)	−0.05	23	9.98	9.07
B0626+24	188.89	6.23	−5(12)	−5(12)	0.24	−53	6.58	11.99
B0628−28	237.03	−16.75	−32(3)	−34.3(12)	−0.42	−226	6.44	12.48
J0633+1746	195.21	4.27	−33(4)	178(4)	0.01	135	5.53	12.21
B0643+80	133.24	26.82	3(3)	18(3)	0.70	118	6.71	12.34
B0656+14	201.18	8.26	17(3)	44(3)	0.04	60	5.05	12.67
B0655+64	151.62	25.23	−1(7)	−10(7)	0.21	−21	9.66	10.07
J0711−6830	279.60	−23.27	−11.6(6)	−10.3(6)	−0.34	−39	9.77	8.46
B0736−40	254.27	−9.18	7(2)	−18.6(15)	−0.42	−230	6.57	11.90
B0740−28	243.85	−2.43	−13.6(2)	−22.6(2)	−0.09	−222	5.20	12.23
B0751+32	188.25	26.72	−8(4)	−1(5)	0.68	−6	7.33	12.10
B0756−15	234.54	7.24	0(5)	4(5)	0.37	55	6.82	12.03

Table 2 – *continued*

PSR	l (°)	b (°)	μ_l (mas yr^{-1})	μ_b (mas yr^{-1})	Z (kpc)	V_Z (km s^{-1})	log[τ_c (yr)]	log[B_s (G)]
B0809+74	140.06	31.61	32.8(4)	34.69(13)	0.23	60	8.09	11.67
B0818−13	235.96	12.61	48(7)	−16(9)	0.43	−147	6.97	12.21
B0820+02	222.06	21.26	5(9)	6(11)	0.37	27	8.12	11.48
B0823+26	197.03	31.75	100(3)	40(3)	0.19	58	6.69	11.98
B0833−45	263.62	−2.77	−42.21(9)	−17.25(8)	−0.01	−24	4.05	12.53
B0834+06	219.79	26.28	−43(4)	30(5)	0.29	83	6.47	12.47
B0835−41	260.98	−0.32	18(3)	−12(3)	−0.01	−91	6.53	12.22
B0906−17	246.19	19.86	54(11)	1(11)	0.31	2	6.98	11.72
B0919+06	225.48	36.40	−64.95(11)	61.69(8)	0.71	282	5.70	12.39
B0950+08	228.97	43.71	−24.23(8)	26.20(8)	0.18	23	7.24	11.39
J1012+5307	160.40	50.85	16.8(2)	15.6(2)	0.32	19	9.69	8.48
J1024−0719	251.77	40.53	27(3)	−70(3)	0.25	−98	9.64	8.50
B1039−19	265.66	33.60	−4(4)	12(4)	0.82	70	7.37	12.06
J1045−4509	280.92	12.27	−1.1(19)	3.5(13)	0.42	32	9.83	8.57
B1112+50	154.46	60.36	17(3)	53(3)	0.39	56	7.02	12.31
B1133+16	241.96	69.21	−338.0(4)	166.0(4)	0.34	101	6.70	12.33
B1237+25	252.45	86.56	−105.92(18)	−44.91(18)	0.86	−11	7.36	12.07
B1257+12	311.41	75.42	39.68(11)	−87.4(2)	0.75	−80	8.94	8.93
B1322+83	121.95	33.66	54(20)	−6(8)	0.42	−18	7.27	11.79
B1325−43	309.95	18.43	17(8)	53(23)	0.42	319	6.45	12.11
B1426−66	312.72	−5.39	−31(5)	−7(4)	−0.09	−33	6.65	12.17
B1449−64	315.80	−4.42	−18.9(10)	−10.7(9)	−0.16	−105	6.02	11.85
J1455−3330	330.80	22.57	22(8)	19(11)	0.20	44	9.72	8.65
B1451−68	313.94	−8.53	−31.2(4)	11.0(4)	−0.07	23	7.63	11.21
B1508+55	91.40	52.27	−16.9(15)	96.0(14)	0.78	276	6.37	12.29
J1518+4904	80.88	54.27	6.5(6)	−7.8(6)	0.51	−14	10.37	9.03
B1534+12	19.94	48.34	−19.517(19)	−12.922(13)	0.71	−39	8.39	9.99
B1541+09	17.90	45.77	−7.2(10)	0.6(10)	2.50	7	7.44	11.76
B1540−06	0.65	36.61	−12(3)	11(3)	0.43	30	7.11	11.90
B1556−44	334.61	6.37	13(9)	10(10)	0.25	108	6.60	11.71
J1603−7202	316.70	−14.49	−2.9(5)	−1.7(5)	−0.29	−9	10.18	8.69
B1600−49	332.22	2.45	−20(6)	19(6)	0.22	459	6.71	11.77
B1604−00	10.80	35.46	−3(11)	−3(13)	0.39	−8	7.34	11.56
B1620−26	351.05	15.96	−26(4)	−7(4)	0.49	−57	8.42	9.44
J1640+2224	41.13	38.26	−10.2(7)	−3.1(4)	0.72	−13	10.25	7.98
J1643−1224	5.75	21.22	−4(5)	−7(4)	0.87	−75	9.60	8.47
B1642−03	14.19	26.06	24.4(16)	20.0(16)	0.49	95	6.54	11.92
J1709+2313	44.60	32.20	−7.3(9)	1.1(8)	0.75	6	10.31	8.12
B1706−16	5.85	13.66	3(13)	−2(11)	0.20	−6	6.21	12.31
J1713+0747	28.83	25.22	0.8(10)	−5.1(6)	0.47	−24	9.93	8.30
B1718−02	20.21	18.93	−20(5)	−11(4)	0.81	−124	7.96	11.30
B1732−07	17.35	13.28	25(3)	17(2)	0.52	179	6.74	11.86
B1737+13	37.16	21.67	−23(3)	13(3)	0.55	85	6.94	12.04
J1744−1134	14.87	9.18	6.2(4)	−17.8(3)	0.06	−30	9.86	8.29
B1749−28	1.61	−0.96	−5(6)	2(6)	−0.02	11	6.04	12.33
B1757−24	5.29	−0.90	−1(9)	−3(9)	−0.08	−74	4.19	12.61
B1804−08	20.14	5.58	0(4)	5(4)	0.27	64	7.95	10.84
B1818−04	25.53	4.73	−1(9)	13(5)	0.16	119	6.18	12.29
B1821+05	35.06	8.85	4(7)	−5(10)	0.28	−43	7.72	11.62
B1821−24	7.87	−5.58	−3.6(16)	−1.2(9)	−0.56	−33	7.48	9.35
B1822−09	21.52	1.32	−12(7)	9(11)	0.02	38	5.37	12.81
B1830−08	23.46	0.06	−2(11)	33(5)	0.00	729	5.17	11.95
B1834−04	27.24	1.12	−6(14)	5(7)	0.10	117	6.53	11.89
B1839+56	86.15	23.80	−23(3)	24(4)	0.68	175	7.24	12.20
B1838−04	27.89	0.27	11(8)	−10(5)	0.03	−269	5.66	12.04

Table 2 – *continued*

PSR	l (°)	b (°)	μ_l (mas yr^{-1})	μ_b (mas yr^{-1})	Z (kpc)	V_Z (km s^{-1})	log[τ_c (yr)]	log[B_s (G)]
B1842+14	45.63	8.14	40(7)	29(10)	0.31	298	6.50	11.93
B1848+13	45.06	6.33	17(9)	9(9)	0.30	114	6.56	11.86
B1855+09	42.36	3.05	−2.94(6)	1.74(5)	0.05	7	9.68	8.50
B1857−26	10.41	−13.45	−50.1(9)	−0.3(5)	−0.47	−3	7.68	11.55
B1900+06	39.89	0.33	11(12)	−1.8(91)	0.05	−72	6.14	12.36
B1902−01	33.76	−3.56	−5(13)	2(8)	−0.37	57	6.52	12.15
B1904+06	40.68	−0.31	8(10)	3(9)	−0.04	118	6.30	11.88
B1905+39	71.02	14.19	19.1(19)	−5(4)	0.55	−51	7.56	11.92
B1907+10	44.91	0.98	1(7)	8(7)	0.07	158	6.23	11.94
J1909−3744	359.80	−19.60	−34.0(7)	−0.5(4)	−0.28	−2	9.52	8.32
J1911−1114	25.21	−9.59	−21(12)	−4(7)	−0.20	−23	9.61	8.36
B1911+13	47.95	1.58	17(7)	−4(7)	0.14	−97	7.01	11.82
B1911−04	31.38	−7.13	2(10)	−8(13)	−0.35	−105	6.51	12.27
B1913+10	44.78	−0.66	8(5)	−6(5)	−0.07	−178	5.62	12.40
B1913+16	50.04	2.11	5.16(7)	2.73(7)	0.22	76	8.03	10.36
B1914+09	44.63	−1.03	10(6)	5(6)	−0.05	70	6.23	11.92
B1924+16	51.93	0.05	9(10)	−16(12)	0.01	−442	5.71	12.51
B1929+10	47.45	−3.90	86.5(3)	−57.41(19)	−0.02	−98	6.49	11.71
B1933+16	52.51	−2.10	−6(3)	−5(3)	−0.21	−133	5.98	12.17
B1935+25	60.91	2.26	20(4)	−7(4)	0.13	−108	6.69	11.56
B1937+21	57.58	−0.30	4.40(2)	0.47(2)	−0.02	8	8.37	8.61
B1937−26	13.97	−21.83	−4(4)	−15(3)	−0.62	−110	6.82	11.80
B1944+17	55.40	−3.51	−4(5)	−4(5)	−0.09	−26	8.46	11.02
B1946+35	70.77	5.03	−1.8(6)	10.7(6)	0.51	293	6.21	12.36
B1951+32	68.84	2.81	−14(4)	17(4)	0.12	201	5.03	11.69
B1953+29	65.91	0.43	1.9(3)	−0.8(3)	0.03	−18	9.51	8.64
B1953+50	84.87	11.54	40(5)	47(5)	0.45	489	6.78	11.93
B1957+20	59.27	−4.71	−26.0(6)	1.1(6)	−0.20	13	9.18	8.22
B2000+40	76.68	5.27	13(7)	−5(7)	0.54	−139	6.92	12.10
B2002+31	69.08	0.01	7(9)	−11(11)	0.00	−391	5.65	13.10
B2011+38	76.00	2.46	−35(3)	13(2)	0.36	523.59	5.61	12.16
B2016+28	68.17	−4.00	−2.5(4)	0.3(3)	−0.07	1.38	7.78	11.46
J2019+2425	64.82	−6.64	−18.40(15)	−1.94(14)	−0.17	−13.61	9.95	8.23
B2020+28	68.93	−4.69	−16.8(4)	−9.3(5)	−0.22	−118.62	6.46	11.91
B2021+51	87.93	8.36	11.1(3)	11.3(3)	0.29	106	6.44	12.11
B2022+50	86.94	7.53	−11(3)	19(3)	0.31	209	6.37	11.99
B2044+15	61.18	−16.85	0(5)	13(6)	−0.70	143	8.00	11.66
B2045−16	30.58	−33.08	42(5)	−107(5)	−0.31	−238	6.45	12.67
J2051−0827	39.26	−30.42	5(3)	−3.8(17)	−0.53	−16	9.75	8.38
B2053+21	67.90	−14.68	5(6)	−3(10)	−0.62	−33	6.98	12.03
B2053+36	79.21	−5.60	5(6)	5(6)	−0.45	109	6.98	11.46
B2106+44	86.98	−2.03	8.0(14)	−1.3(14)	−0.18	−31	7.88	11.28
B2110+27	75.06	−14.04	−51(3)	−17(3)	−0.49	−159	6.86	12.26
B2111+46	89.08	−1.28	−12(13)	−7(13)	−0.10	−150	7.35	11.94
J2124−3358	10.98	−45.44	−40.8(10)	19.4(10)	−0.19	17	9.58	8.51
J2129−5721	338.06	−43.56	−4(3)	−4(3)	−0.94	−19	9.45	8.45
J2145−0750	47.84	−42.09	−9.6(7)	12.1(4)	−0.34	21	9.93	8.85
B2148+63	104.33	7.40	19(4)	−1(4)	0.71	−36	7.55	11.41
B2148+52	97.59	−0.93	−9(3)	0(3)	−0.07	7	5.72	12.27
B2154+40	90.56	−11.36	19.9(9)	−8.4(10)	−0.74	−147	6.85	12.37
B2217+47	98.46	−7.61	−23(8)	−18(7)	−0.29	−188	6.49	12.09
B2224+65	108.71	6.83	185(3)	19(3)	0.22	166	6.05	12.41
J2229+2643	87.77	−26.30	−5(4)	−13(4)	−0.64	−80	10.51	7.82
B2227+61	107.23	3.63	−2(11)	10(11)	0.26	191	6.49	12.00
J2235+1506	80.95	−36.46	21(6)	1(7)	−0.64	2	9.78	9.49

Table 2 – *continued*

PSR	l (°)	b (°)	μ_l (mas yr^{-1})	μ_b (mas yr^{-1})	Z (kpc)	V_Z (km s^{-1})	log[τ_c (yr)]	log[B_s (G)]
B2255+58	108.90	−0.59	−17(5)	−3(5)	−0.05	−64	6.00	12.17
B2303+30	97.79	−26.67	−4(3)	−17(3)	−1.64	−264	6.94	12.33
B2310+42	104.48	−16.44	−20.7(11)	13.6(11)	−0.35	77	7.69	11.30
J2317+1439	91.43	−42.38	5(2)	9(3)	−0.56	26	10.35	7.97
J2322+2057	96.59	−37.32	−22(3)	−6(3)	−0.49	−18	9.89	8.34
B2324+60	113.02	−0.01	18(5)	−7(5)	−0.00	−161	7.02	11.46
B2327−20	49.44	−70.20	37(3)	−60(3)	−0.37	−38	6.75	12.45
B2334+61	114.36	0.22	0(13)	−10(13)	0.01	−149	4.61	12.99
B2351+61	116.31	−0.21	25(3)	1.5(21)	−0.01	24	5.96	12.60

Table 3. Pulsars with parallax measurements. This table contains the name, parallax and distance of each pulsar as measured from the parallax, a reference for the measurement and 2D speed of the pulsar assuming the proper motion given in Table 1 and the distance determination.

PSR	Parallax (mas)	Dist. (kpc)	Ref.	V_T (km s^{-1})
B0329+54	0.94(11)	1.06(12)	1	98(11)
J0437−4715	6.98(19)	0.143(4)	2	94(3)
J0633+1746	6.4(18)	0.16(5)	3	125(40)
B0656+14	3.47(36)	0.29(3)	4	59(7)
B0809+74	2.31(4)	0.433(7)	1	103(2)
B0823+26	2.8(6)	0.36(8)	5	186(42)
B0833−45	3.4(2)	0.29(2)	6	80(5)
B0919+06	0.83(13)	1.20(19)	7	503(80)
B0950+08	3.82(7)	0.262(5)	1	36(1)
B1133+16	2.80(16)	0.36(2)	1	641(36)
B1237+25	1.16(8)	0.86(6)	1	481(33)
B1257+12	1.3(4)	0.8(2)	8	344(90)
B1451−68	2.2(3)	0.45(6)	9	88(12)
J1713+0747	0.9(3)	1.1(4)	10	34(13)
J1744−1134	2.8(3)	0.36(4)	11	36(4)
B1855+09	1.1(3)	0.9(2)	12	27(6)
B1857−26	<1.1	>0.9	13	>219
B1929+10	3.02(9)	0.331(10)	1	177(5)
B2016+28	1.03(10)	0.97(9)	1	31(3)
B2020+28	0.37(12)	2.7(9)	1	310(100)
B2021+51	0.50(7)	2.0(3)	1	120(18)
J2145−0750	2.0(6)	0.5(2)	14	33(9)

References: (1) Brisken et al. (2002), (2) van Straten et al. (2001), (3) Caraveo et al. (1996), (4) Brisken et al. (2003b), (5) Gwinn et al. (1986), (6) Dodson et al. (2003), (7) Chatterjee et al. (2001), (8) Wolszczan et al. (2000), (9) Bailes et al. (1990b), (10) Camilo et al. (1994), (11) Toscano et al. (1999a), (12) Kaspi et al. (1994), (13) Fomalont et al. (1999), (14) Löhmer et al. (2004).

CL02 distance is clearly incorrect and hence, we do not include this pulsar in the remaining analyses presented in this paper.

As the distances predicted by the CL02 electron density model are, on average, smaller than the TC93 model, the derived 2D speeds are also lower (Fig. 2a). For our sample, the mean distance has decreased by ∼2 per cent (the median decrease is ∼10 per cent). According to the TC93 model, four pulsars have 2D speeds $V_T^{TC} >$ 1000 km s^{-1}, whereas, using the CL02 model, only two pulsars (PSRs B2011+38 and B2224+65) have such large 2D speeds. The apparent 2D speeds of the remaining two, PSRs B0523+11 and B2148+63, have decreased to $V_T^{CL} = 446$ and 449 km s^{-1}, respectively.

Table 4. The ten largest distance changes in our sample between the TC93 and CL02 models.

PSR	D^{TC} (kpc)	D^{CL} (kpc)
B0523+11	>7.7	3.1
B0559−05	>7.5	3.9
B0736−40	>11.0	2.6
B0835−41	4.2	1.1
B1552−31	>6.1	2.3
B1737+13	>4.8	1.5
B1802−07	11.6	5.0
B1900−06	8.8	5.4
B2011+38	13.1	8.4
B2148+63	>13.7	5.5

In passing, we note that the CL02 model places pulsars at distances almost halfway between the Lyne, Manchester & Taylor (1985) model (that was commonly used prior to the TC93 model) and the TC93 model (Fig. 2b). For the remainder of this paper we use the CL02 model (unless independent distance estimates exist), but caution that, even with this most recent distance model, the distances to some pulsars, and hence their velocities, may be significantly under- or overestimated. We therefore emphasize the importance of continuing to measure pulsar distances to refine future electron density models.

4 ONE- AND TWO-DIMENSIONAL SPEEDS

For all pulsars in our sample at least one component of their space velocity is determined. We make use of these by defining 1D speed $V_1 = \mu D$ of a pulsar, where μ is the proper motion in either the longitudinal or latitudinal direction and D is the distance obtained using the CL02 model. For 156 pulsars we can obtain their 2D speeds $V_2 = \mu_{tot} D$, where μ_{tot} is the total proper motion. In what follows, we investigate aspects of the 1D and 2D speeds obtained for the sample as a whole and in various subsets of the sample.

4.1 Statistical overview

A summary of the 1D and 2D speeds for various subsets of the complete sample is given in Table 5. Histograms of the data are

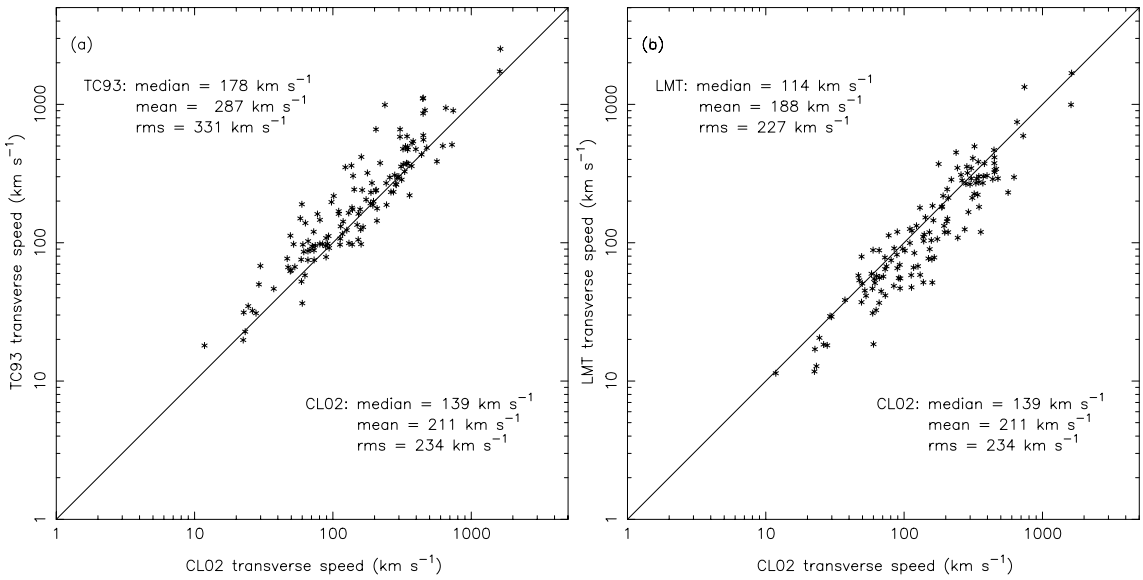

Figure 2. Comparison between pulsar 2D speeds obtained using the CL02 model with: (a) the TC93 model; (b) the Lyne et al. (1985) model.

Table 5. Parameters for different samples of pulsars. The top half of the table provides values for 1D speeds, the bottom half contains 2D speeds. $N^1_{\rm psr}$ and $N^2_{\rm psr}$ indicate the number of pulsars for which 1D and 2D speeds have been measured. The $N^1_{\rm psr}$ pulsars provide N_S 1D velocity components. The table provides mean and median speeds ($\bar{V}$, $V^{\rm med}$), distances ($\bar{D}$, $D^{\rm med}$)) and characteristic ages ($\bar{\tau}_{\rm c}$, $\tau_{\rm c}^{\rm med}$) and an estimate of the mean space velocity V_3 obtained from the 1D and 2D speeds; see text.

	All	Normal	Recycled	SNR	$\tau_{\rm c} < 3$ Myr	$\tau_{\rm c} > 3$ Myr	$D < 500$ pc
$N^1_{\rm psr}$	217	178	39	8	73	105	19
N_S	372	299	73	15	119	180	36
$\bar{V}_1$ (km s^{-1})	133(8)	152(10)	54(6)	150(42)	192(20)	126(10)	77(17)
$V_1^{\rm med}$ (km s^{-1})	79	100	38	95	123	85	54
$\bar{D}$ (kpc)	2.36(12)	2.58(14)	1.32(19)	2.4(6)	3.3(3)	2.06(13)	0.35(2)
$D^{\rm med}$ (kpc)	1.91	2.14	0.95	2.25	2.79	1.83	0.36
$\bar{\tau}_{\rm c}$ (Myr)	1376	70.7	7333	0.1	1.2	118.9	1719
$\tau_{\rm c}^{\rm med}$ (Myr)	7.4	4.3	5610	0.07	1.1	14.1	37
$\bar{V}_3 = 2\bar{V}_1$ (km s^{-1})	266(16)	304(20)	108(12)	300(82)	384(40)	252(20)	154(34)
$N^2_{\rm psr}$	156	121	35	7	46	75	17
$\bar{V}_2$ (km s^{-1})	211(18)	246(22)	87(13)	227(85)	307(47)	209(19)	128(33)
$V_2^{\rm med}$ (km s^{-1})	139	178	73	142	240	152	94
$\bar{D}_2$ (kpc)	2.25(15)	2.50(17)	1.4(2)	2.7(7)	3.0(3)	2.18(17)	0.35(2)
$D_2^{\rm med}$ (kpc)	1.70	2.07	1.04	2.5	2.10	1.99	0.36
$\bar{\tau}_{c,2}$ (Myr)	1732	59.8	7511	0.06	1.1	95.7	1565
$\tau_{c,2}^{\rm med}$ (Myr)	8.7	4.82	5210	0.04	0.9	10.2	18
$\bar{V}_3 = (4/\pi)\bar{V}_2$	269(23)	313(28)	111(17)	289(108)	391(60)	266(24)	163(42)

presented in Figs 3 and 4. Table 5 contains a description of each subset, the number of pulsars within this set, the number of measured velocity components (for the 1D speeds, this is less than twice the number of pulsars as some pulsars have only a proper motion measurement in one coordinate) and average distances and characteristic ages.

The mean 1D speed is 133(8) km s^{-1} and the fastest moving pulsar in our sample, PSR B2011+38, has $V_1 = 1284$ km s^{-1} in right ascension and 996 km s^{-1} in declination. The smallest upper limit is $V_1 < 2$ km s^{-1} in right ascension for PSR J1640+2224. The 2D speeds range from 12 km s^{-1} for PSR B1706−16 to 1625 km s^{-1} for PSR B2011+38. The mean 2D speed is 211(18) km s^{-1}, or 269(25) km s^{-1} with the TC93 model. This latter value is consistent with 300(30) km s^{-1} obtained by Lyne & Lorimer (1994) who also used the same distance model.

4.2 Isotropy of the velocity vector

The observed 1D and 2D speeds we measure are, of course, the projection of the 3D space velocity of the pulsar. For an isotropically distributed pulsar velocity vector of magnitude V_3, it is straightforward to show that the mean 1D and 2D speeds are given by $V_3/2$ and $\pi V_3/4$, respectively. A simple test of isotropy, then, is to compare the ratios of the mean 2D and 1D speeds which should be $\langle V_2\rangle/\langle V_1\rangle = \pi/2 \simeq 1.57$. For the sample as a whole, we find $\langle V_2\rangle/\langle V_1\rangle = 1.6(2)$ in excellent agreement with an isotropic velocity vector. Indeed, all

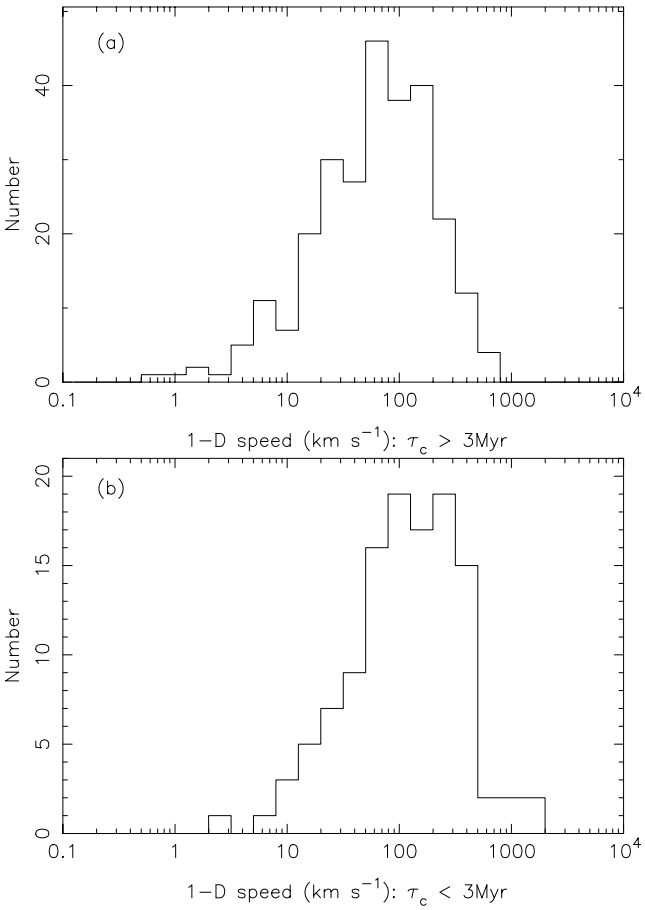

Figure 3. 1D speeds for pulsars in our sample that: (a) have characteristic ages greater than 3 Myr; (b) have characteristic ages less than 3 Myr.

the subsamples in Table 5 give similar results. This simple but important result will be used to derive the 3D velocity distribution in Section 6.

4.3 High-velocity pulsars

The highest 2D speeds in our sample are 1624, 1608 and 740 km s^{-1} for PSRs B2011+38, B2224+65 and B1830−08 respectively.[4] As there is a large gap between the second and third fastest objects, we must consider whether the speeds greater than 1000 km s^{-1} are real or due to inaccuracies either in the distance model or in the proper motion measurements. If the true 2D speed of PSR B2011+38 were 1000 km s^{-1} then the observed proper motion would be 25 mas yr^{-1} for its estimated distance of 8 kpc. This required proper motion is significantly lower than recent Very Large Array measurements by Brisken et al. (2003a) who obtain $\mu_{\rm tot} = 40(2)$ mas yr^{-1} and from Paper I where we measured $\mu_{\rm tot} = 51(10)$ mas yr^{-1}. We can therefore rule out the proper motion measurements being in error. However, as there are no independent distance estimates to either PSR B2011+38 or B2224+65 it is possible that the reported distances may be overestimated (the reported distance to PSR B2011+38 of 8.4 kpc is the largest in our sample).

If these 2D speeds are correct, then it means that the fastest pulsars are still part of a long tail in the velocity distribution with the gap between them and the slower-moving pulsars being caused by small number statistics (i.e. pulsars at the high end of the distribution are rare and so the gap is only an artefact) and do not make up a separate population of high-velocity objects. To investigate whether this is possible, we undertook a simple simulation where we approximated Fig. 2 by a single 2D speed distribution. In three out of 15 Monte Carlo realizations of the sample, we found a gap above and below 1000 km s^{-1}. We therefore conclude that the gap observed in Fig. 2 is entirely consistent as being the result of small-number statistics of sampling a continuous velocity distribution with a large tail.

To confirm these high 2D speeds will require independent distance measurements. However, the observed bow shock for PSR B2224+65 does suggest a high velocity for this pulsar which is most likely greater than 800 km s^{-1} (see Cordes, Romani & Lundgren 1993; Chatterjee & Cordes 2004).

4.4 Young and old pulsars

After selecting only those pulsars with characteristic ages less than 3 Myr (Fig. 4b), we obtain a mean 2D speed of 307(47) km s^{-1}, consistent with the value of 345(70) km s^{-1} obtained by Lyne & Lorimer (1994) who estimated distances using the TC93 model. The mean 2D speed for young pulsars is higher than the value of 209(19) km s^{-1} for older, non-recycled pulsars; see Fig. 4(d). However, the velocity distributions for the young and older pulsars appear to overlap. We note that the sample of 46 young pulsars contains nine objects with 2D speeds less than 100 km s^{-1} and only seven with 2D speeds >400 km s^{-1}. The smallest 2D speed, 12 km s^{-1}, is measured for PSR B1706−16, although whether this represents a truly low-velocity population or a projection effect is not clear. We investigate this issue further in Section 6.

4.5 Pulsar–supernova remnant associations

It is notable that the 1D and 2D speeds for the eight pulsars that have been associated with supernova remnants (see Tables 5 and 6) are significantly lower than the mean for other young pulsars and consistent with the mean for the entire pulsar sample that includes both young and old pulsars. In contrast, by inferring 2D speeds based on the offset of pulsars from the centre of the supernova remnant, Frail, Goss & Whiteoak (1994) suggested that most pulsars in supernova remnants have velocities that are significantly larger than the mean. More recent proper motion measurements show that some of the velocities claimed by Frail et al. are too high. For example, PSR B1757−24 was thought to be in G5.4−1.2, giving rise to a 2D speed which was predicted to be 1800 km s^{-1} but which has subsequently been shown to be ∼100 km s^{-1}, so that it is unlikely to be associated with the supernova remnant (Gaensler & Frail 2000; Thorsett, Brisken & Goss 2002). Other pulsars with 2D speeds predicted by Frail et al. to be greater than 1000 km s^{-1} are PSRs B1509−58, B1610−50, B1800−21 and B1930+22. Unfortunately these pulsars glitch regularly and it is difficult to obtain proper motions using timing techniques. Interferometric measurements of these pulsars are therefore highly desirable.

One explanation for the observed low velocities of pulsars associated with supernova remnants is that any high-velocity objects

[4] These are the observed 2D speeds of the pulsars. After removing the effects of Galactic rotation and the peculiar motion of the Sun, the 2D speeds in the local standard of rest of the pulsar become 1459, 1640 and 730 km s^{-1}, respectively.

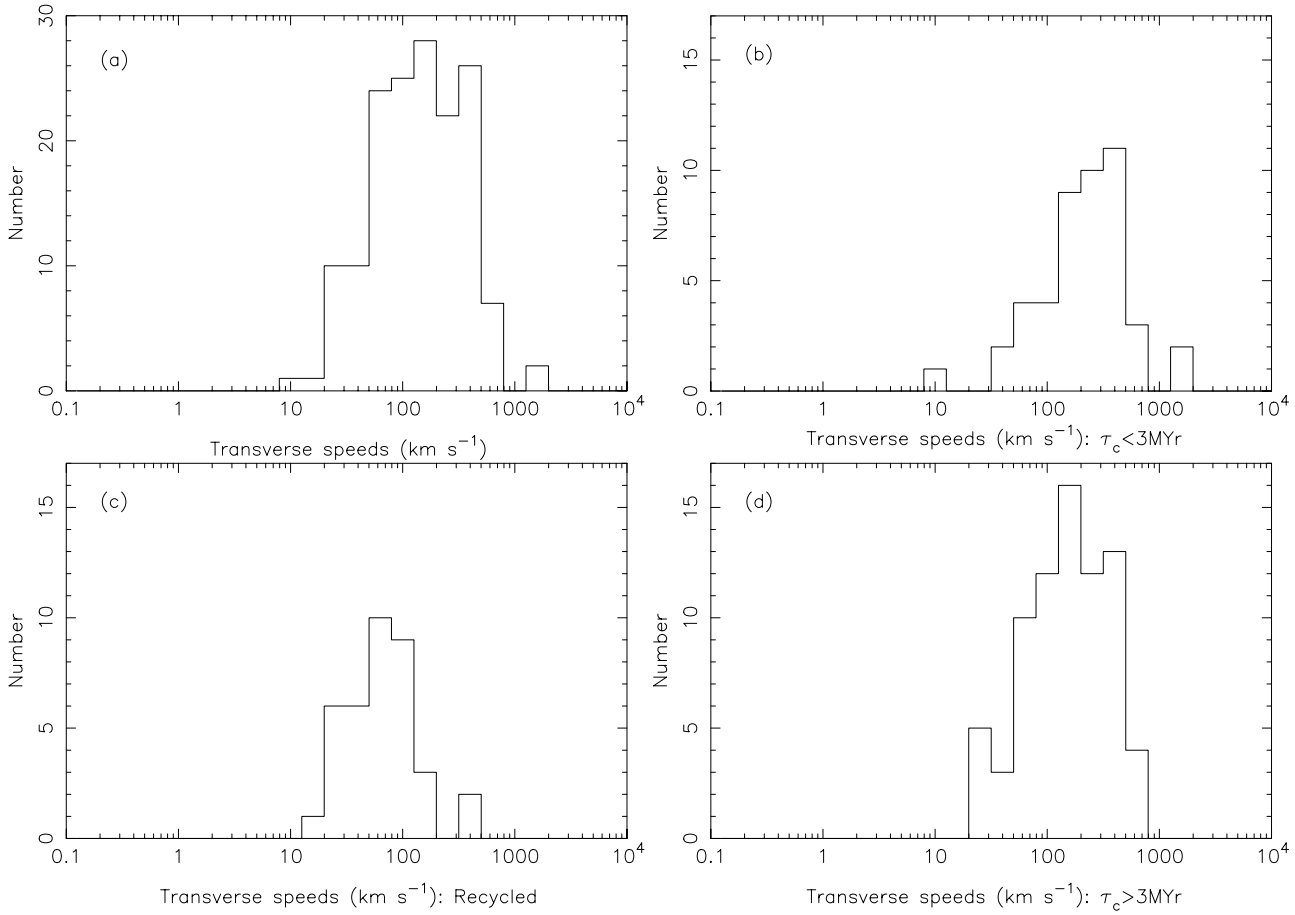

Figure 4. 2D speeds for: (a) all the pulsars in our sample; (b) pulsars with characteristic ages less than 3 Myr; (c) recycled pulsars; (d) normal (not recycled) pulsars with characteristic ages greater than 3 Myr. The mean 2D speeds for each sample are 211(18), 307(47), 87(13) and 209(19) km s^{-1}, respectively. Panels b, c and d are drawn to the same scale.

Table 6. Pulsars in our sample that have been associated with supernova remnants. Recent work (e.g. Thorsett et al. 2002) indicates that PSR B1757−24 is not associated with G5.4−1.2 as was previously thought. For PSR J0538+2817 only one component of velocity has been determined.

PSR	SNR	τ_c (kyr)	V_T (km s^{-1})
B0531+21	Crab	1.24	140
J0538+2817	S147	618	>140
B0656+14	Monogem Ring	111	59
B0833−45	Vela	11.3	80
(B1757−24)	(G5.4−1.2)	(15.5)	(89)
B1830−08	W41	41	740
B1951+32	CTB80	10.7	300
B2334+61	G114.3+0.3	40.9	159

would leave the central regions of the remnant within a short timescale and are therefore hard to detect in a targeted search of a supernova remnant. The difficulty in identifying a genuine association is additionally compounded by the fact that the probability of a chance association with a pulsar increases with the square of the angular offset from the remnant centre. One possible example of a high-velocity pulsar associated with a supernova remnant is PSR B1830−08 (nominally the third fastest object in our sample with $V_T^{CL} = 740$ km s^{-1}) and the shell supernova remnant W41 (Clifton & Lyne 1986; Gaensler & Johnston 1995). Regardless of the distance uncertainties, the new proper motion measurement for PSR B1830−08 presented in Paper I shows that the pulsar is moving away from W41 and is consistent with birth within the boundaries of the remnant. Further observations to constrain the distance and origin of this young pulsar are required.

In Table 6 we include an association between PSR B2334+61 and G114.3+03 which was first suggested by Kulkarni et al. (1993) and Fürst, Reich & Seiradakis (1993). Fürst et al. found that the ages and distances of both objects are comparable and that the pulsar is located close to the centre of the remnant. They also noted that, assuming the 41 kyr characteristic age to be a good indicator of the true age of the pulsar, the expected proper motion from birth in the centre of the supernova remnant to the current position of the pulsar should be $\mu_{tot} = 12(2)$ mas yr^{-1}. Our timing measurement of $\mu_{tot} = 11(13)$ mas yr^{-1} is consistent with the predicted value for an association. Clearly, given the large uncertainty in μ_{tot}, we cannot rule out that the pulsar was not born in the centre of the supernova remnant. We can state, however, that B2334+61 was born somewhere within G114.3+0.3 (even with a proper motion of $\mu_{tot} = 24$ mas yr^{-1}, the pulsar would only have moved ∼16 arcmin or only 25 per cent of the current diameter of the supernova remnant within 41 kyr). The birth position of B2334+61 will be determined more accurately with a few more years of timing data or by making interferometric measurements.

4.6 Recycled pulsars

In Table 7 we list the 2D speeds for the recycled pulsars in our sample. The mean value of $V_T = 87(13)\,\mathrm{km\,s^{-1}}$ is entirely consistent with the value of $85(13)\,\mathrm{km\,s^{-1}}$ reported by Toscano et al. (1999b) using the TC93 model. This consistency is due to the known millisecond pulsars being relatively close by and so CL02 and TC93 agree much better than they do for more distant pulsars. Also, a parallax has been measured for many of these pulsars providing independent distance estimates (for the millisecond pulsars, only the predicted distances to PSRs J0218+4232, J1045−4509, J1643−1224, J2129−5721 and J2317+1439 have changed by more than 1 kpc from the TC93 to the CL02 model).

Table 7. 2D speeds for the recycled pulsars. For binary systems, the orbital period P_b is also given. The orbital period listed for PSR B1257+12 is that of the most massive planet; see text.

PSR	V_T ($\mathrm{km\,s^{-1}}$)	P_b (d)
J0034−0534	79	1.59
J0218+4232	63	2.03
J0437−4715	94	5.74
J0613−0200	59	1.19
J0621+1002	23	8.31
J0711−6830	89	–
J0751+1807	>1†	0.26
J1012+5307	49	0.60
J1022+1001	>35†	7.81
J1024−0719	150	–
J1045−4509	72	4.08
B1257+12	345	66.5
J1455−3330	63	76.2
J1518+4904	28	8.63
B1534+12	113	0.42
J1603−7202	47	6.31
J1640+2224	73	176
J1643−1224	103	147
J1709+2313	68	22.7
J1713+0747	34	67.8
J1730−2304	>50†	–
J1744−1134	36	–
J1804−2717	>7†	11.1
B1855+09	27	12.3
J1909−3744	80	1.53
J1911−1114	139	2.72
B1913+16	73	0.32
B1937+21	14	–
B1953+29	84	117
B1957+20	359	0.38
J2019+2425	160	76.5
J2051−0827	26	0.10
J2124−3358	63	–
J2129−5721	52	6.63
J2145−0750	33	6.84
J2229+2642	117	93.0
J2235+1506	91	–
J2317+1439	31	2.46
J2322+2057	95	–

†For these pulsars, only the proper motion coordinate in ecliptic longitude has been measured. The given value is therefore a lower limit to its 2D speed.

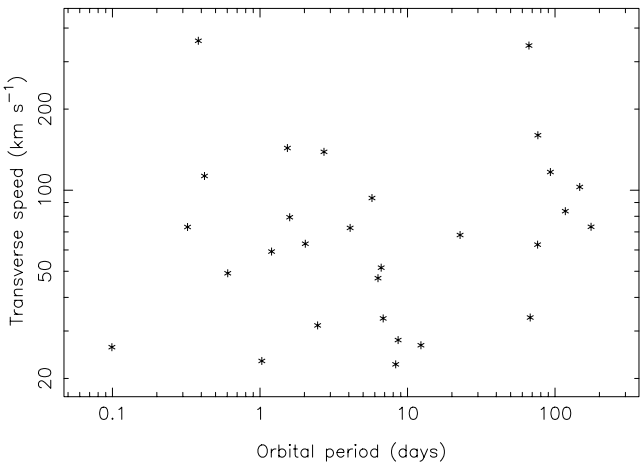

Figure 5. 2D velocity versus orbital period for binary millisecond pulsars.

Toscano et al. (1999) also noted that isolated millisecond pulsars have lower velocities than binary millisecond pulsars (see also Johnston, Nicastro & Koribalski 1998). Our sample contains seven solitary and 28 binary millisecond pulsars with measured 2D speeds. The size of this sample more than doubles that of Toscano et al. (1999). The mean 2D speeds we obtain for the solitary and binary millisecond pulsars are 77(16) and 89(15) $\mathrm{km\,s^{-1}}$, respectively, which are not significantly different.

Tauris & Bailes (1996) predicted that the velocities of binary millisecond pulsars should increase with decreasing orbital period. No such correlation was found in their data which they attributed to selection effects. Our data, shown in Fig. 5, also show no correlation. Tauris & Bailes (1996) predict a lower limit for the velocity of such pulsars of $\approx$25 $\mathrm{km\,s^{-1}}$ and an upper limit of $\approx$270 $\mathrm{km\,s^{-1}}$. Two pulsars in our sample, PSRs B1257+12 and B1957+20, with 2D speeds of 344 and 359 $\mathrm{km\,s^{-1}}$ respectively, are clearly well above this upper limit. The first, PSR B1257+12 is known to be part of a planetary system and may have undergone a different evolution than other binary millisecond pulsars. The second, the 'black-widow' pulsar PSR B1957+20, is thought to be slowly ablating its companion (Fruchter, Stinebring & Taylor 1988) and may, therefore, provide a link between binary and isolated millisecond pulsars. This seems rather unlikely because we do not see solitary millisecond pulsars with such high velocities.

We may expect double neutron star systems to have even lower velocities than millisecond pulsars as a consequence of having survived two supernova explosions. Unfortunately, we currently only have three double neutron star systems with proper motion determinations. Our proper motion measurement for PSR J1518+4904 from Paper I of 25(7) $\mathrm{km\,s^{-1}}$ agrees well with 28(2) $\mathrm{km\,s^{-1}}$ found by by Nice, Taylor & Sayer (1999) (only the uncertainties in the total proper motion were considered when determining the errors on these values). Earlier measurements for PSR B1534+12 and B1913+16 imply respective 2D speeds of 113.0(1) and 73(2) $\mathrm{km\,s^{-1}}$, respectively. More recently, from scintillation measurements of the double pulsar J0737−3039, Coles et al. (2004) derive a 2D speed of $\sim$66 $\mathrm{km\,s^{-1}}$. A proper motion measurement of this system should

be available soon through both interferometric and timing measurements. Given the small-number statistics, we simply note that these 2D speeds are entirely consistent with the distribution for the whole sample of recycled pulsars.

5 MOTION IN THE GALACTIC PLANE

Standard models of pulsar birth suggest that pulsars are born in Type II supernovae (see, for example, Gunn & Ostriker 1970). The progenitor massive stars lie along the Galactic plane with a scale-height of ∼63 pc (Sun & Han 2004). Any velocity kick imparted to the pulsar at its birth will make it move away from the Galactic plane. Hence, the motion of young pulsars that appear to be moving toward the plane can only be explained by projection effects or by the pulsar being born well above the plane and out of the expected progenitor region. For instance, the unknown radial motion of a pulsar may make it appear to be moving towards the plane when it is, in fact, moving away (see, for example, Helfand & Tademaru 1977). Restricting our study to pulsars with characteristic ages less than 3 Myr guarantees that all bound objects are within the first quarter-cycle of their oscillation perpendicular to the Galactic plane (see, for example, Cordes & Chernoff 1998).

Harrison et al. (1993) found that the positions and proper motions of PSRs B0450−18, B0523+11, B0540+23 and B1718−02 could only be explained by the pulsars being born above the Galactic plane and currently moving moving toward the plane. However, Cordes & Chernoff (1998) analysed the proper motions of 49 pulsars with characteristic ages less than 10 Myr and found that all were consistent with the earlier conclusion of Helfand & Tademaru (1977) that all pulsars are born in the plane and subsequently move away. The main difference between the analyses was that Harrison et al. (1993) defined a much smaller progenitor region than Cordes & Chernoff (1998). For instance, even though PSR B0540+23 is likely to be moving towards the Galactic plane, owing to its low height above the Galactic plane of only 0.2 kpc, it was deemed, by Cordes & Chernoff (1998), to have been born within the expected pulsar progenitor region of the Galaxy.

In our sample, only PSR B0114+58 (and B0540+23; see above discussion) has a characteristic age less than 3 Myr, a current z height greater than 100 pc and is seemingly moving toward the plane. However, this pulsar lies below the plane at a distance of 130 pc which is within current estimates of the pulsar progenitor scaleheight. We therefore agree with Cordes & Chernoff (1998) that all the pulsars that seem to be moving toward the plane are consistent with having been born within the plane.

In Fig. 6 we indicate the angle of velocity vectors with respect to the Galactic plane for pulsars with Galactic latitudes less than 30°. The lengths of the tracks are indicative of the magnitude of the pulsar velocities and were calculated using the pulsar proper motions in Galactic longitude and latitude only; as before, the radial velocity component has been ignored. We find no predominant angle for the motion of the pulsars with respect to the Galactic plane.

Earlier we analysed pulsar velocities based on proper motion measurements in celestial or ecliptic coordinates. The difference between these velocities and those obtained after the effects of Galactic rotation and the peculiar motion of the Sun have been removed is minimal and is smaller than the likely uncertainties due to the pulsar distances. The shape of the 2D speeds after taking into account the effects of Galactic rotation is little changed from the earlier version (the mean velocities are identical). However, the velocities for a few pulsars change significantly. For instance, in the most extreme case the velocity of PSR B1933+16 reduces from 346 to 208 km s^{-1}.

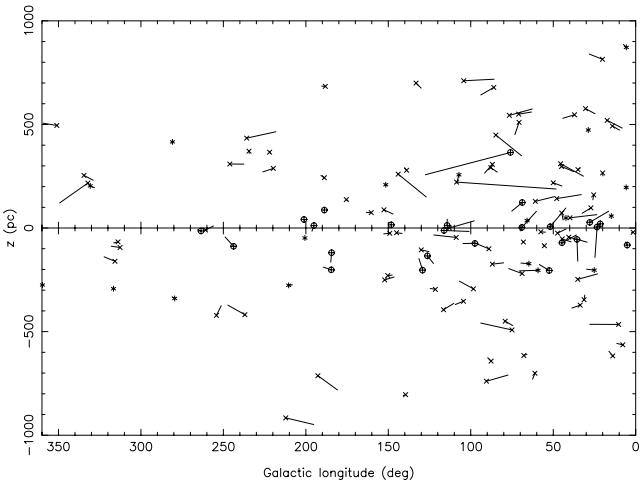

Figure 6. The motion of pulsars with respect to the Galactic plane. Pulsars indicated by a circle have $\tau_c < 1$ Myr, those with $\tau_c > 1$ Gyr by a '*' symbol. All other pulsars are indicated using a '×' symbol.

6 THREE-DIMENSIONAL VELOCITIES OF YOUNG PULSARS

With the exception of two binary pulsars (Bell et al. 1995; van Kerkwijk, Bergeron & Kulkarni 1996) it is generally not possible to make a direct measurement of the true 3D space velocity of a pulsar. However, as the observed data are consistent with an isotropic velocity vector, it is possible to determine the 3D speed distribution from the observed 1D and 2D speeds. In this section we describe and discuss the consequences of a new technique that deconvolves the expected form of a single-magnitude isotropic space velocity from the observed 1D and 2D distributions.

6.1 The deconvolution technique

Following Lyne & Lorimer (1994), we derive the birth velocity distribution using the sample of pulsars with $\tau_c < 3$ Myr to minimize any selection biases against detecting older high-velocity pulsars. The resulting samples of 119 1D and 46 2D speeds therefore represent two projected views of the underlying 3D distribution which we seek to recover. For a single-magnitude isotropic space velocity distribution of V_3, the probability density function corresponding to a logarithmic bin V_1 for 1D speeds

$$P(V_1)\,\mathrm{d}\log(V_1) = \frac{V_1}{V_3}\,\mathrm{d}\log(V_1) \qquad (0 < V_1 < V_3). \tag{1}$$

Similarly, for the 2D case we find

$$P(V_2)\,\mathrm{d}\log(V_2) = \frac{V_2^2}{V_3}\frac{\mathrm{d}\log(V_2)}{\left(V_3^2 - V_2^2\right)^{1/2}} \qquad (0 < V_2 < V_3). \tag{2}$$

One way to think about these 1D and 2D distributions is that they represent the convolution of the underlying 3D distribution with the 1D and 2D probability density functions. We therefore can use a CLEAN-type algorithm Hogböm (1974) to deconvolve these functions from the observed speed distributions. In detail, we (i) cross-correlate the analytic expression with the observed distribution to determine the velocity, V_3, corresponding to the maximum correlation; (ii) subtract a scaled version of the analytic expression defined by V_3 from the observed distribution with a small gain factor;

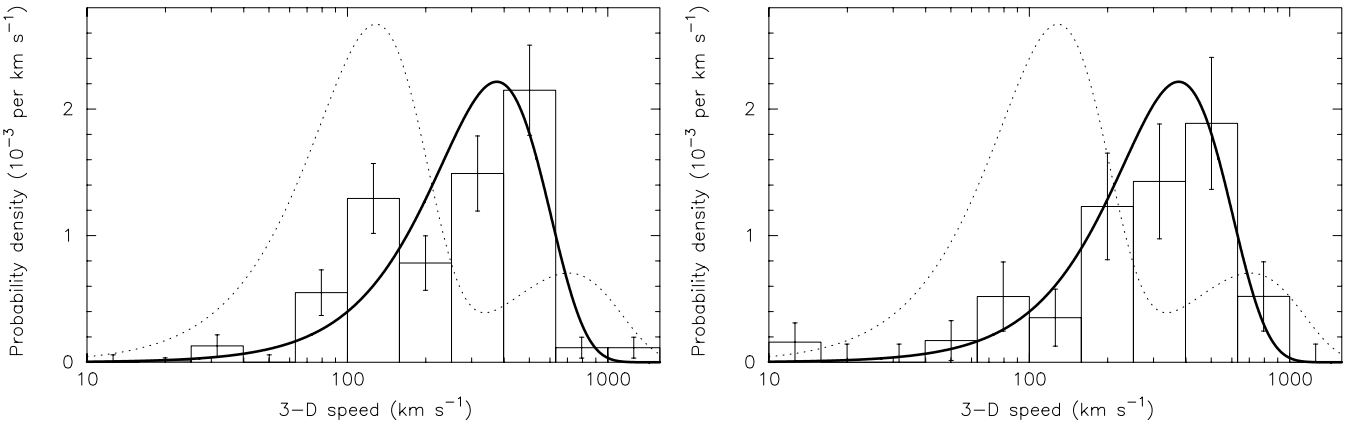

Figure 7. The 3D velocity distributions obtained from the observed 1D (left) 2D (right) distributions using the deconvolution technique described in the text. The uncertainties on each histogram bin are calculated as $\sqrt{N}$ where N is the number of pulsars in each bin. The histograms are normalized to unit area. The dotted curve shows the 3D distribution favoured by Arzoumanian et al. (2002). The solid curve is the best-fitting Maxwellian distribution to the histogram from the 2D distribution with $\sigma = 265$ km s^{-1}.

(iii) record a 'CLEAN' component corresponding to V_3 and repeat for a large number of iterations. The 'CLEAN' components are subsequently binned to give a histogram representing the true 3D space velocities.

6.2 The underlying space velocity distribution

The resulting 3D distributions obtained from the 1D and the 2D observed distributions are shown in Fig. 7. Both forms of the 3D distribution are in excellent agreement with each other and have mean 3D speeds of 400(40) and 431(60) km s^{-1}, respectively. The smaller error on the mean derived from the 1D speeds reflects the larger size of this sample. It is notable that the long 'tail' towards low speeds in the observed 1D histogram (Fig. 3b) is not present in the 3D histogram. This reflects the fact that the observed 'tail' is simply due to projection effects. Our 3D distributions show that very few young pulsars have 3D speeds less than $\sim$60 km s^{-1}. The right panel of Fig. 7 shows that an excellent fit (reduced $\chi^2 = 0.6$) can be obtained using a simple Maxwellian distribution with a 1D rms $\sigma = 265$ km s^{-1}.

We have tested our deconvolution algorithm by simulating 3D velocity distributions of different forms, randomly selecting as many 1D speeds as in our real sample from these 3D distributions, binning the resulting 1D speeds as in Fig. 3 and using our deconvolution method to derive the underlying 3D velocities. In all cases, we have successfully reproduced the original form of the simulated distribution. It is of particular interest to determine whether a single component velocity distribution could be obtained using our algorithm from a simulated bimodal 3D distribution. We have therefore formed a bimodal 3D distribution from two Gaussians of differing amplitudes centred on 100 and 630 km s^{-1} similar to that proposed by Arzoumanian, Chernoff & Cordes (2002). Using the technique described above, we attempted to derive a 3D distribution using our deconvolution method. In all cases we reproduced a bimodal distribution. The zero-lag cross correlation between the predicted and the simulated distributions provided a measure of the goodness of the reproduced distribution. All the correlation coefficients were found to be close to 1 implying that the deconvolution technique accurately reproduces the bimodal distribution, the positions of the components and their relative amplitudes. Similar results are obtained when simulating a single component distribution.

6.3 Comparison with earlier work

Although most authors agree that a broad spectrum of velocities is required to explain the observations, considerable disagreement exists on whether the distribution has more than one component. Based on a number of available constraints, Fryer, Burrows & Benz (1998) favour a bimodal velocity distribution with one peak near 0 km s^{-1} and another above 600 km s^{-1}. Similarly, from an extensive study of a sample of pulsars detected in low-frequency ($\sim$0.4 GHz) radio surveys, Arzoumanian et al. (2002) find a two-component distribution with characteristic velocities of 90 and 500 km s^{-1}. Whether the origin of these two components is due to a physical effect of the kick mechanism is still a matter for debate.

The results of our novel deconvolution analysis of a large sample of pulsars do not support the idea of a bimodal distribution of pulsar velocities. This can be seen in the left panel of Fig. 7 where we compare our results with an appropriately normalized version of the 3D distribution preferred by Arzoumanian et al. (2002). This figure clearly shows that the new distribution is incompatible with the Arzoumanian et al. model which predicts an excess of low-velocity pulsars and dearth of high-velocity ones. Fryer et al. (1998) argued that the pulsar proper motion data available to them at that time were not sufficient to constrain distribution of neutron star kick velocities. It would be instructive (but beyond the scope of this paper) to repeat their calculations using the larger sample of proper motions now available. For now, we re-iterate that a Maxwellian distribution provides an excellent fit to the 3D pulsar velocity distribution.

An earlier analysis by Hansen & Phinney (1997) on a smaller sample of pulsars also preferred a Maxwellian distribution for V_3. However, their value of $\sigma = 190$ km s^{-1} does not provide a very good fit (reduced $\chi^2 = 5.7$) to the new larger sample presented here. Our results, however, do agree well with the mean velocity of 450(90) km s^{-1} found by Lyne & Lorimer (1994). The larger sample of pulsars in this analysis has resulted in a reduction of the uncertainties by more than a factor of 2. The slight reduction in the mean value of 400(40) km s^{-1} compared with Lyne & Lorimer (1994) is largely a result of the smaller average distances inferred from the CL02 model compared with TC93.

The different pulsar velocity distributions proposed predict different fractions of pulsars that will escape the Galactic gravitational potential. Assuming the escape velocity of our Galaxy to be $\sim$430 km s^{-1} (Leonard & Tremaine 1990), we find that 35 per cent

of all pulsars will escape the Galactic potential in the new distribution compared to 50 per cent for the bimodal distribution of Arzoumanian et al. (2002) and only 16 per cent for the Hansen & Phinney (1997) distribution.

In summary, our new results on the 3D pulsar velocity distribution more closely match the earlier conclusions of Lyne & Lorimer (1994) than the results of Hansen & Phinney (1997), Fryer et al. (1998) or Arzoumanian et al. (2002). While we have tried to account for selection effects by placing a 3 Myr cut-off in our sample of young pulsars, a more detailed analysis that fully takes into account the various selection effects present in this new sample (and ideally including the other constraints discussed by Fryer et al. 1998) should now be carried out to further investigate the results presented here.

7 CONCLUSIONS

We have presented an updated catalogue of the kinematics of 233 pulsars, effectively doubling the size of the previous sample. Our results may be summarized as follows.

(i) In contrast to the results of Frail et al. (1994), most pulsars within supernova remnants are found to have lower velocities than other pulsars. This is most likely due to selection effects where fast moving pulsars leave the supernova shell within a relatively short period of time.

(ii) The proper motions for PSRs B1830−08 and B2334+61 are consistent with their proposed associations with the supernova remnants W41 and G114.3+0.3.

(iii) The fastest moving pulsar with a well-defined distance is PSR B1133+16 which has a 2D speed of 640 km s^{-1}. However, according to the CL02 (and TC03) distance model PSRs B2011+38 and B2224+65 both have 2D speeds greater than 1500 km s^{-1}.

(iv) The CL02 distance model generally predicts smaller distances, and hence 2D speeds, than the TC03 model. The mean 1D and 2D speeds for pulsars with characteristic ages less than 3 Myr are 192(20) and 307(47) km s^{-1}. The observed 1D and 2D speeds clearly demonstrate that the 3D velocity vector is isotropic.

(v) Based on a deconvolution analysis of the new samples of 1D and 2D speeds of young pulsars, we find the mean 3D birth speed to be 400(40) km s^{-1}. The 3D speeds are well fit by a Maxwellian distribution with 1D rms $\sigma = 265$ km s^{-1}. We find no evidence for a bimodal velocity distribution.

The implications of these results for 'kick' mechanisms may be summarized by stating that the true space velocities of young pulsars range from a few tens to well over 1000 km s^{-1} with a mean velocity of 400(40) km s^{-1}. According to Lai et al. (2001): (1) local convective instabilities in the collapsed stellar core can account for velocities up to ∼100 km s^{-1}; (2) global asymmetric perturbations can create velocities over 1000 km s^{-1}; (3) asymmetric neutrino emission can provide kick velocities up to ∼1000 km s^{-1}; (4) the electromagnetic rocket effect can accelerate pulsars up to similarly high velocities. Our results suggest that (1) is unlikely. (4) is testable by studying the alignment between the direction of motion of a pulsar and its spin axis (see Deshpande, Ramachandran & Radhakrishnan 1999) although the duration of the kick will also affect the observed alignment (Spruit & Phinney 1998).

More proper motions will become available within the next few years both from interferometry and from timing. The Jodrell Bank data archive will be able to provide values or limits on the proper motions of many hundreds of pulsars in the near future. These will further improve the constraints on the distribution and origin of pulsar velocities.

ACKNOWLEDGMENTS

During the course of this work we made extensive use of NASA's Astrophysics Data System bibliographic data base and the astro-ph preprint service. DRL is a University Research Fellow funded by The Royal Society.

REFERENCES

Arzoumanian Z., Fruchter A. S., Taylor J. H., 1994, ApJ, 426, L85
Arzoumanian Z., Chernoff D. F., Cordes J. M., 2002, ApJ, 568, 289
Bailes M., Manchester R. N., Kesteven M. J., Norris R. P., Reynolds J. E., 1990a, MNRAS, 247, 322
Bailes M., Manchester R. N., Kesteven M. J., Norris R. P., Reynolds J. E., 1990b, Nat, 343, 240
Bell J. F., Bessell M. S., Stappers B. W., Bailes M., Kaspi V. M., 1995, ApJ, 447, L117
Brisken W. F., Benson J. M., Goss W. M., Thorsett S. E., 2002, ApJ, 571, 906
Brisken W. F., Fruchter A. S., Goss W. M., Herrnstein R. M., Thorsett S. E., 2003a, AJ, 126, 3090
Brisken W. F., Thorsett S. E., Golden A., Goss W. M., 2003b, ApJ, 593, L89
Camilo F., Foster R. S., Wolszczan A., 1994, ApJ, 437, L39
Camilo F., Nice D. J., Taylor J. H., 1996, ApJ, 461, 812
Caraveo P. A., Bignami G. F., Mignani R., Taff L. G., 1996, ApJ, 461, L91
Chatterjee S., Cordes J. M., 2004, ApJ, 600, L51
Chatterjee S., Cordes J. M., Lazio T. J. W., Goss W. M., Fomalont E. B., Benson J. M., 2001, ApJ, 550, 287
Chatterjee S., Cordes J. M., Vlemmings W. H. T., Arzoumanian Z., Goss W. M., Lazio T. J. W., 2004, ApJ, 604, 339
Clifton T. R., Lyne A. G., 1986, Nat, 320, 43
Cognard I., Lestrade J.-F., 1997, A&A, 323, 211
Cognard I., Bourgois G., Lestrade J. F., Biraud F., Aubry D., Darchy B., Drouhin J. P., 1995, A&A, 296, 169
Coles W. A., McLaughlin M. A., Rickett B. J., Lyne A. G., Bhat N. D. R., 2005, ApJ, 623, 392
Cordes J., Chernoff D., 1998, ApJ, 505, 315
Cordes J. M., Lazio T. J. W., 2002, astro-ph/0207156 (CL02)
Cordes J. M., Lazio T. J. W., 2003, astro-ph/0301598
Cordes J. M., Romani R. W., Lundgren S. C., 1993, Nat, 362, 133
Dehnen W., Binney J., 1998, MNRAS, 298, 387
Deshpande A. A., Ramachandran R., Radhakrishnan V., 1999, A&A, 351, 195
Dodson R., Legge D., Reynolds J. E., McCulloch P. M., 2003, ApJ, 596, 1137
Doroshenko O., Löhmer O., Kramer M., Jessner A., Wielebinski R., Lyne A. G., Lange C., 2001, A&A, 379, 579
Fomalont E. B., Goss W. M., Manchester R. N., Lyne A. G., 1997, MNRAS, 286, 81
Fomalont E. B., Goss W. M., Beasley A. J., Chatterjee S., 1999, AJ, 117, 3025
Frail D. A., Weisberg J. M., 1990, AJ, 100, 743
Frail D., Goss W., Whiteoak J., 1994, ApJ, 437, 781
Freire P. C., Camilo F., Kramer M., Lorimer D. R., Lyne A. G., Manchester R. N., D'Amico N., 2003, MNRAS, 340, 1359
Fruchter A. S., Stinebring D. R., Taylor J. H., 1988, Nat, 333, 237
Fryer C., Burrows A., Benz W., 1998, ApJ, 496, 333
Furst E., Reich W., Seiradakis J., 1993, A&A, 276, 470
Gaensler B. M., Johnston S., 1995, MNRAS, 275, L73
Gaensler B. M., Frail D. A., 2000, Nat, 406, 158
Gunn J. E., Ostriker J. P., 1970, ApJ, 160, 979
Gwinn C. R., Taylor J. H., Weisberg J. M., Rawley L. A., 1986, AJ, 91, 338
Hansen B., Phinney E. S., 1997, MNRAS, 291, 569
Harrison P. A., Lyne A. G., Anderson B., 1993, MNRAS, 261, 113

Helfand D., Tademaru E., 1977, ApJ, 216, 842
Hobbs G., Lyne A. G., Kramer M., Martin C. E., Jordan C. A., 2004, MNRAS, 353, 1311 (Paper I)
Hogböm J., 1974, A&AS, 15, 417
Jacoby B. A., Bailes M., van Kerkwijk M. H., Ord S., Hotan A., Kulkarni S. R., Anderson S. B., 2003, ApJ, 599, L99
Johnston S., Nicastro L., Koribalski B., 1998, MNRAS, 297, 108
Kaspi V. M., Taylor J. H., Ryba M., 1994, ApJ, 428, 713
Kerr F. J., Lynden-Bell D., 1986, MNRAS, 221, 1023
Konacki M., Wolszczan A., Stairs I. H., 2003, ApJ, 589, 495
Kramer M. et al., 2003, MNRAS, 342, 1299
Kulkarni S. R., Predehl P., Hasinger G., Aschenbach B., 1993, Nat, 362, 135
Lai D., Chernoff D. F., Cordes J. M., 2001, ApJ, 549, 1111
Lange C., Camilo F., Wex N., Kramer M., Backer D., Lyne A., Doroshenko O., 2001, MNRAS, 326, 274
Leonard P. J. T., Tremaine S., 1990, ApJ, 353, 486
Lewandowski W., Wolszczan A., Feiler G., Konacki M., Soltysiński T., 2004, ApJ, 600, 905
Löhmer O., Kramer M., Driebe T., Jessner A., Mitra D., Lyne A. G., 2004, A&A, 426, 631
Lyne A. G., Lorimer D. R., 1994, Nat, 369, 127
Lyne A. G., Anderson B., Salter M. J., 1982, MNRAS, 201, 503
Lyne A. G., Manchester R. N., Taylor J. H., 1985, MNRAS, 213, 613
McGary R. S., Brisken W. F., Fruchter A. S., Goss W. M., Thorsett S. E., 2001, AJ, 121, 1192
Manchester, R. N., Hobbs, G. B., Teoh, A., Hobbs, M., 2005, AJ, 129, 1993
Migliazzo J. M., Gaensler B. M., Backer D. C., Stappers B. W., van der Swaluw E., Strom R. G., 2002, ApJ, 567, L141
Nice D. J., Taylor J. H., 1995, ApJ, 441, 429
Nice D. J., Taylor J. H., Sayer R. W., 1999, in Arzoumanian Z., van der Hooft F., van den Heuvel E. P. J., eds, Pulsar Timing, General Relativity, and the Internal Structure of Neutron Stars. North Holland, Amsterdam, p. 74
Nice D. J., Splaver E. M., Stairs I. H., 2001, ApJ, 549, 516
Odenkirchen M., Brosche P., Geffert M., Tucholke H. J., 1997, New Astron., 2, 477
Olling R. P., Merrifield M. R., 1998, MNRAS, 297, 943
Siegman B. C., Manchester R. N., Durdin J. M., 1993, MNRAS, 262, 449
Splaver E. M., Nice D. J., Arzoumanian Z., Camilo F., Lyne A. G., Stairs I. H., 2002, ApJ, 581, 509
Spruit H., Phinney E. S., 1998, Nat, 393, 139
Sun X., Han J., 2004, MNRAS, 350, 232
Tauris T. M., Bailes M., 1996, A&A, 315
Taylor J. H., Cordes J. M., 1993, ApJ, 411, 674 (TC93)
Thorsett S. E., Arzoumanian Z., Camilo F., Lyne A. G., 1999, ApJ, 523, 763
Thorsett S. E., Brisken W. F., Goss W. M., 2002, ApJ, 573, L111
Toscano M., Britton M. C., Manchester R. N., Bailes M., Sandhu J. S., Kulkarni S. R., Anderson S. B., 1999a, ApJ, 523, L171
Toscano M., Sandhu J. S., Bailes M., Manchester R. N., Britton M. C., Kulkarni S. R., Anderson S. B., Stappers B. W., 1999b, MNRAS, 307, 925
van Kerkwijk M. H., Bergeron P., Kulkarni S. R., 1996, ApJ, 467, L89
van Straten W., 2003, PhD thesis, Swinburne University of Technology
van Straten W., Bailes M., Britton M., Kulkarni S. R., Anderson S. B., Manchester R. N., Sarkissian J., 2001, Nat, 412, 158
Webbink R. F., 1985, in Goodman J., Hut P., eds, Proc. IAU Symp. 113, Dynamics of Star Clusters, Reidel, Dordrecht, p. 541
Weisberg J. M., Taylor J. H., 2003, in Bailes M., Nice D. J., Thorsett S., eds, Radio Pulsars. Astron. Soc. Pac., San Francisco, p. 93
Wolszczan A. et al., 2000, ApJ, 528, 907
Wyckoff S., Murray C. A., 1977, MNRAS, 180, 717

This paper has been typeset from a TEX/LATEX file prepared by the author.